DESK COPY

JOURNAL OF GEOPHYSICAL RESEARCH, VOL. 96, NO. B9, PAGES 14,509–14,528, AUGUST 10, 1991

Geophysical Log Responses and Their Correlation With Bed-to-Bed Stress Contrasts in Paleozoic Rocks, Appalachian Plateau, New York

RICHARD A. PLUMB

Schlumberger-Doll Research, Ridgefield, Connecticut

KEITH F. EVANS[1]

Lamont-Doherty Geological Observatory, Palisades, New York

TERRY ENGELDER

Department of Geosciences, Penn State University, University Park, Pennsylvania

A 1-km profile of in situ stress and geophysical log data was acquired in the Wilkins well to study the relationship between rock properties and in situ stress contrasts. The Wilkins well penetrates Devonian clastic rocks on the Appalachian Plateau near the town of South Canisteo, New York. Open hole hydraulic fracture stress measurements were made in stratigraphic sequences where geophysical logs indicated significant bed-to-bed variations in elastic and lithologic properties. Analysis of stress magnitudes and interval-averaged geophysical data shows that principal horizontal stress magnitudes correlate directly with elastic stiffness and inversely with clay content. A similar relation is found for older Paleozoic strata penetrated by a well at Auburn, New York. Correlations between stress magnitude and geophysical properties observed in the Wilkins and Auburn wells provide strong evidence that bed to bed stress variations arise from a uniform ENE-WSW directed strain acting on beds of different Young's modulus rather than from variations in rock shear strength. Because of their high Young's modulus, sandstones, siltstones, and limestones in the northern Appalachian Basin are likely to be stronger barriers to hydraulic fracture propagation than shales. Porosity logs in the Wilkins well show that the large decrease in horizontal stress found at the base of the Rhinestreet Formation occurs where shales are less compacted. The correlation with undercompaction is consistent with a paleo-overpressure drainage mechanism as the cause for the stress decrease.

INTRODUCTION

Closely spaced stress measurements in the same borehole indicate that stress magnitudes in sedimentary rocks can vary from bed to bed [*Warpinski et al.*, 1983; *Evans et al.*, 1989*a*]. Such bed-to-bed variation in the least principal horizontal total stress S_h favors propagation of natural joints in the lower stressed beds [e.g., *Engelder*, 1985] and acts to prevent joints initiated in the lower stress beds, from propagating into beds of higher stress. This phenomenon is exploited by petroleum engineers to contain hydraulic fractures within beds of low stress [*Nolte*, 1982]. A precise knowledge of differences in stress magnitude allows engineers to predict the type of fracture treatment that will assure containment in the reservoir beds [*Simonson et al.*, 1978; *Warpinski et al.*, 1982; *Smith*, 1985]. However, precise stress magnitude data are rarely obtained in shales. Instead it is commonly assumed that the least principal horizontal total stress in shales is greater than in adjacent reservoir rocks. This paper presents quantitative information about stress magnitudes and geophysical properties of siltstone-shale-limestone sequences where S_h in shales is less than in adjacent strata. Such stress variations are not widely recognized but may be common in tectonically mature basins where rocks have undergone significant postdiagenetic deformation and are currently subjected to a significant component of deviatoric horizontal compression. Low stress in shales also conflicts with simple Earth stress models based on gravitational loading and lateral confinement boundary conditions [*Anderson et al.*, 1972; *Jaeger and Cook*, 1976; *Johnson*, 1986; *Thiercelin and Plumb*, 1991]. A better understanding of the mechanisms responsible for bed-to-bed stress variations will improve our understanding of the origin and distribution of natural fractures and the propagation of commercial hydraulic fractures.

Reservoir rocks are commonly sandstones bounded above and below by shale. The difference between S_h in the sandstone and S_h in the shale is dependent on the present tectonic state of the basin, the pore pressure, and the mechanical properties of the sandstone and shale. Young basins, which are still subsiding, are often tectonically relaxed, and a significant component of horizontal deviatoric tension is often present. In relaxed basins, S_h in shale is typically closer to S_V than in adjacent sandstone beds. Such behavior is attributed to the tendency for shale to creep toward a state of lithostatic stress (i.e., $S_h = S_H = S_v$) [cf. *Warpinski*, 1986]. Therefore we refer to a stress profile through a basin where S_h for shale is greater than S_h for sandstone as a relaxed-state profile. Older basins, particularly those which are presently subjected to a significant component of horizontal deviatoric compression, may be distinguished by a higher average S_h (i.e., S_h close to or

[1]Now at Institute of Geophysics, Swiss Federal Institute of Technology, ETH-Honggerberg, Zurich, Switzerland.

Paper number 91JB00896.
0148-0227/91/91JB-00896$05.00

exceeding S_v) and an S_h in shale which is lower than in adjacent sandstone or limestone. In these basins, higher compressive stress develops in those beds with greater elastic moduli (i.e., sandstones and limestones). We define a stress profile where S_h is greater in elastically stiffer strata as a compressed-state profile. This paper documents two examples of compressed-state profiles on the Appalachian Plateau, New York.

Advances in our understanding of stress magnitudes in sedimentary rocks have come primarily from in situ stress measurements [*Breckels and van Eekelen*, 1982; *Kry and Gronseth*, 1983; *Hickman et al.*, 1985; *Warpinski et al.*, 1983; *Warpinski*, 1986; *Whitehead et al.*, 1986; *Evans et al.*, 1989*a*]. Vertical profiles of S_h commonly show considerable variation within a single well, in addition to the usual increase of magnitude with depth. Little is known about the causes for most of these variations because stress and lithology data are rarely sufficiently complete to show systematic correlations between the two. Several studies in sedimentary rock which combine geophysical log data with stress measurements provide evidence that variations in the depth trend of S_h are correlated with clay content as indicated by gamma ray logs. Measurements in the MWX-2 well, located near Rifle, Colorado, provide one of the earliest and best documented examples of a relaxed-state stress profile [*Warpinski*, 1982; *Warpinski et al.*, 1983]. The greatest S_h magnitudes are measured in high Poisson's ratio shales bounding lower stress, lower Poisson's ratio sandstones. *Warpinski* [1986] attributes these lithology-dependent stress variations to pore pressure variations and inelastic deformation. Other relaxed-state profiles have recently been documented in the Staged Field Experiment (SFE) wells located in east Texas [*Whitehead et al.*, 1986]. A drawback with the cased-hole stress measurement technique used in the MWX and SFE studies is that it provides S_h data over an interval of uncertain vertical extent. Uncertainty about vertical extent raises questions about which intervals were actually fractured and if several beds were fractured how uniform is S_h over the region intersected by the hydrofracture. *Kry and Gronseth* [1983] have published limited data which are consistent with a compressed-state profile in the Esso-Elmsworth well, Alberta, Canada. Their data included two cased-hole stress measurements and a gamma ray log in a sand-shale sequence where S_h in shale is lower than in an adjacent sandstone. Another example of a compressed-state profile was found in a well located in Auburn, New York. Comparison of open hole stress measurements reported by *Hickman et al.* [1985] and geophysical log data reported by *Plumb and Singer* [1983] shows that stress magnitudes are lower in shales and siltstones than in sandstone and are inversely proportional to Poisson's ratio.

Given the considerable scientific and practical importance of stress variations in the upper crust, it is clearly relevant to identify the tectonic and lithologic factors that give rise to compressed-state stress profiles. Recently, *Evans et al.* [1989*a*] reported a detailed set of open hole stress measurements in sedimentary rocks of the Appalachian Basin, near the town of South Canisteo, New York, and about 120 km southwest of Auburn, New York (Figure 1). The majority of measurements were made in the Wilkins well and sample stress to a depth of 1 km in Devonian rocks. The Auburn measurements sample underlying older Paleozoic rocks. The large number of closely spaced stress measurements made in the Wilkins well shows clear evidence of bed-to-bed variations of stress magnitude which correlate with lithologic variations. *Evans et al.* [1989*b*] examined the mechanical properties of cores for equivalent stratigraphic units recovered from a 20-km distant well (NY1; Figure 1). They inferred that stiffer beds tended to host higher stress a result which was explained by elastic shortening of the crust [*Plumb et al.*, 1987]. A comprehensive suite of geophysical logs was run in the Wilkins well to complement the stress measurements. This paper presents the geophysical log data and analyzes them with a view of clarifying the lithologic factors that govern the observed stress variations. Finally, this data set confirms the existence of a compressed-state stress profile in the Wilkins well and strengthens the suggestion that such a profile is also represented by the Auburn data. The combined Wilkins and Auburn data provide constraints on the origin of the compressed-state stress profile in the Appalachian Basin.

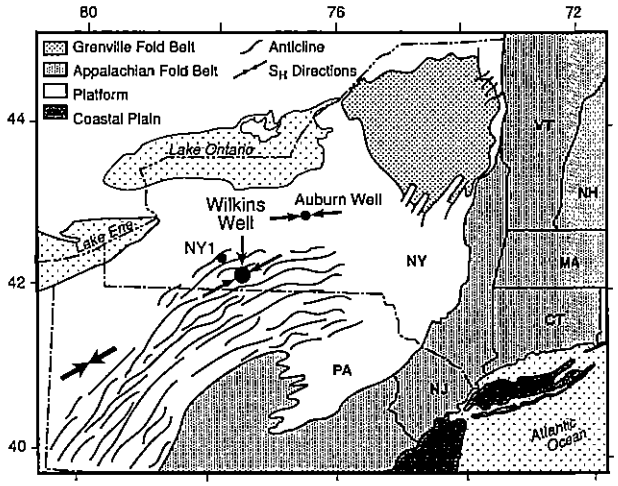

Fig. 1. Geologic sketch map showing the location of the Wilkins, Auburn, and NY1 wells. Directions of the contemporary maximum horizontal stress S_H measured in the Wilkins and Auburn wells are shown by small arrows. The bold arrow (lower left) gives the average S_H direction for the Appalachian Basin [after *Plumb and Cox*, 1987].

Previous publications gave detailed information about the stress measurement program and a geological analysis of the origin of stress variations found at the Wilkins site [*Evans et al.* 1989*a*, *b*] and are not repeated. Two key features of the Wilkins stress profile that will be the subject of much attention are (1) stress measured in shales is always lower than in adjacent sandstones or limestones and (2) a significant decrease in horizontal stress occurs at a depth of about 720 m.

THE WILKINS WELL EXPERIMENT

Tectonic Setting

The Wilkins well is located on the Appalachian Plateau near the town of South Canisteo, in western New York (Figure 1). The Appalachian Plateau is an allochthonous sheet detached within the Silurian Salts below the Devonian section penetrated by the well. Splay faults emanating from the salt decollement cut up into Devonian section to terminate as blind thrust faults in shales above the Tully lime-

TABLE 1. Geophysical Logs Deployed in the Wilkins Well Giving a Simplified Description of Each Tool's Measurement and Some Applications

Logging Tool	Measurement	Application
Digital BHTV-BTT	Ultrasonic pulse-echo scanner, digitizes reflected amplitude and two-way transit time.	Oriented reflectance and transit time images of fractures, bedding, and wellbore breakouts.
Compensated neutron tool-CNT	Irradiates rock with high energy neutrons. Measures flux of thermal neutrons.	Concentration of hydrogen atoms in pore fluids and minerals, reported as neutron porosity ϕ_n. Detect porous rock, estimate porosity, estimate relative concentraion of hydroxyls associated with clays.
Dual laterolog tool-DLL	Measures potential difference between two electrodes while passing focused current into rock.	Deep (LLd) and shallow (LLs) reading electrical resistivity R_a (Ω m). Indicates resistivity of pore fluid and responds to cation exchange capacity of minerals.
High-resolution dipmeter tool-HDT	Four oriented-orthogonal measurements of electrode current, inclinometer and two orthogonal calipers.	Microconductivity curves: determine dip of bedding planes; Calipers: determine borehole geometry, detect breakouts; Inclinometer: give borehole attitude in three dimensions.
Lithology density tool-LDT	Irradiates formation with γ rays, measures flux and energy spectrum of back scattered γ rays.	Determine bulk density (ρ_b), photoelectric absorption factor (P_e), and porosity (ϕ_d); estimate lithology using ρ_b and P_e.
Long spacing sonic tool-LSS	Excites elastic waves in rock, digitizes waveforms.	Determine compressional and shear wave slowness of rock; used to estimate Poisson's ratio ν; used with ρ_b to estimate Young's modulus E, bulk modulus K_b, shear modulus G.
Microelectrical scanner tool-MST	Prototype array-electrode device used to make microconductivity measurements.	Oriented high-resolution electric image of borehole surface, images bedding planes, sedimentary structure, and small fractures.
Natural gamma ray spectroscopy tool-NGT	Records natural γ radioactivity in three energy windows.	Detect shales, estimate clay types. Measures total radioactivity SGR (API); derive concentrations of potassium K, uranium U, and thorium Th. Derive a U-free radioactivity log, CGR.

See text for more on log interpretation.

stone. Blind thrusts are expressed at the surface by a series of gentle folds with limb dips of less than about 2° [*Wedel*, 1932; *Engelder and Geiser*, 1980]. Low dips expected at this site are confirmed by borehole imagery and bedding dips of less than 5° computed from a dipmeter log (Table 1). Contemporary stress directions in the Appalachian Basin are well documented. Hydrofracture and borehole breakout data indicate an ENE-WSW orientation for the maximum horizontal principal stress [*Plumb and Cox*, 1987; *Zoback and Zoback*, 1989]. Stress orientations determined in the vicinity of the Wilkins well are consistent with the regional stress field [*Evans et al.*, 1989*a*; *Hickman et al.*, 1985] (Figure 1). Regional data also indicate that a discontinuity in the depth trend of stress magnitudes occurs at the base of the Devonian section, coincident with the salt. Stress ratios (S_h/S_v) in Devonian sands and shales typically approach or exceed unity, whereas stress ratios below the salt are typically of the order of 0.65 [*Evans*, 1989].

The Wilkins well penetrates prodeltaic Devonian sedimentary rocks consisting predominantly of alternating sequences of black and gray mudstone/siltstone turbidities. Limestone beds are common in the section below the West River member of the Genesee Formation. Above the Cashaqua Formation of the Sonyea Group, occasional thin (<15 m) quartz-rich beds, constitute the only interruption to the monotonous clay-rich mudstones and siltstones (Figure 2). Following *Van Tyne* [1982], the major lithologies encountered, upward from the bottom of the well, are (Figure 2) Tully Limestone, a fine-crystaline or micritic limestone with few fossils; bituminous black shales of the Geneseo, Lodi, Pen Yan, and West River members of the Genesee Formation; gray shales and black shales of the Cashaqua and Middlesex formations of the Sonyea Group and inhomogeneous black shales of the Angola and Rhinestreet formations of the West Falls Group. The color of the shales reflects their organic content where the highest organic content is found in black shales. The Angola and Rhinestreet shales are interbedded with dirty-fine sandstones and siltstones with a shaly matrix. Thicker quartz-rich siltstone beds are identified by D–K in Figure 2. To be consistent with *Evans et al.* [1989*a*, *b*], we refer to these quartz-rich siltstone beds as "sands." With the exception of the K sand, locally known as the Grimes sandstone, "sand" beds are rarely continuous over tens of square kilometers [*Evans et al.*, 1989*a*, *b*]. Composition and texture determined from thin section analysis of cores samples from NY1 show that the Grimes sandstone contains about 35–40% quartz. Grain size is poorly sorted with about 30% of grains measuring less than 15 μm and about 5% of grains measuring 100 μm or greater (very fine sand to medium silt). The Cashaqua and Rhinestreet formations are dominated by clays. Grain size is well sorted with 90% of grains measuring less than 15 μm (medium silt to clay) [*Evans et al.*, 1989*b*].

Geophysical Logs

A comprehensive suite of geophysical well logs was run to locate physically different lithologic units prior to making stress measurements (Table 1). Well logs distinguish the major lithologic units on the basis of their geophysical signature. Inferences about variations in composition and texture of the Devonian rocks is based upon the assumption

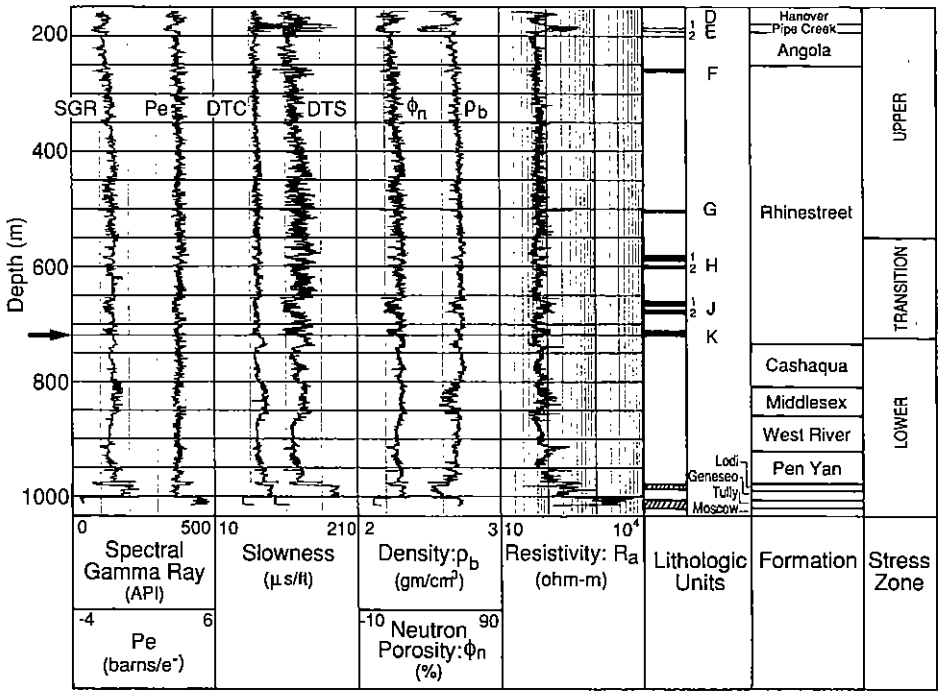

Fig. 2. The principal geophysical logs from the Wilkins well showing key lithologic units, formations names and the three stress zones. "Sands" interbedded in shales are indicated by D–K. The Lodi and Tully limestones are located at the base of the well. An arrow in the depth track shows the location of the stress decrease at the base of the K sand.

that the physics governing tool response developed for clay bearing reservoir rocks is approximately correct. The following is a brief description of the well logs and how we interpret their measurements in Devonian shales. A comprehensive treatment of the measurement physics and tool configurations is given by *Ellis* [1987].

Electrical resistivity log. The apparent electrical resistivity R_a of Devonian rocks was measured by the deep reading laterolog (LLd). The units of R_a are ohm meter^2/meter or ohm meter. Resistivity is determined by measuring the potential difference between an electrode on the sonde and another located at the surface of the Earth, while a focused current flows from the sonde into the formation. The variation of the potential is directly proportional to resistivity of the formation. In shaly sands, electrical conductivity, the reciprocal of resistivity, depends upon the conductivity of the pore fluids, the tortuosity of the pore space and surface conductance between contacting clay minerals [*Sen*, 1987]. Models of the conductivity of fluid-saturated clay-bearing rocks express rock conductivity as the sum of two components: the conductivity of formation water and the surface conductance due to the presence of clay-bound water [*Waxman and Smits*, 1968; *Clavier et al.*, 1984]. In low-porosity Devonian shales we expect conductivity to be dominated by surface conductance. The contribution to conductivity from clay minerals is parameterized by the cation exchange capacity per unit volume Q_v. Conductivity increases as Q_v increases for a given saturating fluid. We interpret decreased R_a as an increase in surface conduction associated with greater volume fraction of inter-connected clay particles.

Spectral gamma ray log. Spectral gamma ray logs measure the natural radioactivity of the rock. One of their primary uses is to distinguish shales from reservoir rocks. We used a tool (NGT) which measures the flux of gamma rays at three energies corresponding to the decay of ^{40}K, ^{238}U, and ^{262}Th, respectively. The tool is calibrated in an artificial shale formation to give mass concentrations of potassium, K in percent; uranium, U in ppm; and Thorium, Th in ppm. The sum of these three components is the total radioactivity which is reported as the spectral gamma ray log, SGR, in API units. The dominant source of radioactivity in sedimentary rocks is due to the decay of ^{40}K. Feldspars are the dominant source of potassium in sandstones, and illite and glauconite are the primary sources in shales. In contrast, Th- and U-bearing minerals are rare. Organic rich shales are recognized by their relatively high concentration of uranium which is absorbed by animal or plant material incorporated in the shale. Because of its high solubility, uranium is easily transported from the clay lattice and may later be precipitated as uranium salts in pores and fractures located some distance from the source rock. A uranium-free radioactivity log, CGR, is obtained by subtracting the U signal from the total radioactivity. The CGR log provides a better representation of the relative clay mineral abundance by eliminating the contributions from organics and uranium salts. Spectral gamma ray data effectively discriminate the three major shale groups in this well and place constraints on clay types.

Bulk density log. Bulk density ρ_b (g/cm^3) is used to estimate bulk porosity and overburden stress. Because of topography in the vicinity of the Wilkins well, overburden stress is slightly less than the vertical stress S_v [cf. *Evans and Engelder*, 1989]. Bulk density is measured by a tool that irradiates the formation with γ rays. The measurement principle is based on the fact that the γ ray counting rate of a detector varies exponentially with the bulk density of the formation. From a measurement of the counting rate and analysis of the γ ray energy spectrum recorded by a set of

TABLE 2. Values of Bulk Density ρ_b and Photoelectric Absorption Factor P_e for Selected Sedimentary Minerals and Rocks

Mineral/Rock	ρ_b, g/cm^3	P_e, b/el
Quartz	2.654	1.806
Orthoclase	2.52	2.86
Anorthite	2.74	3.13
Albite	2.59	1.68
Calcite	2.71	5.084
Dolomite	2.88	3.14
Siderite	3.89	14.69
Illite	2.52	3.45
Chlorite	2.76	6.30
Glauconite*	2.54	16.24
Pyrite	4.99	16.97
Anthracite	1.47	0.16
Clean Sandstone*	2.31	1.75
Dirty Sandstone*	2.39	2.70
Average Shale*	2.65	3.42

*Values are variable; illustrative values are shown [*Ellis*, 1987].

detectors ρ_b and the photoelectric absorption factor P_e (barns per electron) are determined. P_e is sensitive to the average atomic number of rock forming elements and therefore is used to determine basic lithology: sandstone, limestone, or shale (Table 2). Bulk density is used to estimate porosity ϕ_d, shear modulus G, Young's modulus E, and bulk modulus K_b (see the appendix). In conjunction with spectral gamma ray data, P_e helps to further constrain clay types.

Neutron porosity log. Neutron porosity logs are used to identify porous rocks and to estimate their porosity. Neutron tools irradiate the formation with high-energy neutrons. These neutrons are efficiently converted to low-energy thermal neutrons by collisions with atoms of nearly equal mass such as a hydrogen atoms associated with pore water, clay-bound water, or hydrocarbons. The volume fraction of hydrogen atoms in the formation can be estimated from the spatial distribution of thermal neutrons measured by a pair of detectors given a matrix lithology and assuming that hydrogen is volumetrically the dominant element affecting the neutron energy loss. Count rates are large when hydrogen concentration is low. Although some trace elements found in shales may efficiently reduce thermal neutron count rates, the reduction of count rates is dominated by hydroxyls associated with the clay mineral structure [*Ellis*, 1987]. Since there is no standard calibration for shales, we report the count rate data as neutron porosity ϕ_n assuming the rock is a water-filled limestone. The choice of limestone porosity is purely conventional and is not important here since we interpret the variation of ϕ_n in Devonian shales as a relative indicator of clay-bound water or clay content. Void space or porosity in the shales is best estimated by the density porosity ϕ_d. Both porosity estimates are similar in the clay-free Tully limestone.

Acoustic logs. Acoustic logs measure the travel time of compressional and shear waves. A monopole source emits a pulse which excites compressional (p) and shear (s) waves in the rock. Waveforms are recorded by a series of receivers located between 3 and 3.7 m from the source. Digitized waveforms are then processed to extract the p wave and s wave slownesses, DTc and DTs (μs/ft). DTc and DTs are then converted to velocity V_p and V_s (km/s). Interval-averaged elastic moduli are estimated from V_p, V_s, and ρ_b data using equations for elastic solids given in the appendix. Poroelastic corrections to the calculated moduli are not made in this study because rock composition, fluid type, fluid saturation, and porosity, required by the theory, are not accurately known [*Biot*, 1956; *Gassmann*, 1951]. *Geertsma* [1961] has shown that these corrections are small for rocks with porosity as low as those studied here.

In subsequent discussions we distinguish principal logs from derived logs. Principal logs refer to relatively unprocessed data such as resistivity logs and elastic wave slowness logs. A derived log, such as the shear modulus, is a function of two principal logs, density and shear wave slowness. Figure 2 shows the principal geophysical logs. The "sands" and limestones are readily distinguished from the shales on the neutron, density, and slowness logs. A distinct change in curve character can be seen on the γ ray, elastic wave slowness, and neutron logs at the base of the K sand. The change is such that measurements deeper than 720 m appear to be low-pass filtered. High vertical resolution (1 cm) ultrasonic reflectance and electrical conductivity images from the BTT and MST (Table 1) show that the filtered appearance occurs where beds are thinner than the vertical resolution of the conventional logging tools, about 60 cm. This change in bed thickness and log character coincides with a significant stress decrease observed in the Wilkins well and its two neighbors, the O'Dell and Appleton wells [*Evans et al.*, 1989*a*]. The stress decrease occurs near the base of the Catskill delta sequence: a stratigraphic position that was shown by *Engelder and Oertel* [1985] to separate normally compacted delta sediments from undercompacted shales below.

Stress Profile

A total of 43 open hole stress measurements were made in the Wilkins well by a wire line deployed hydrofracturing system [*Evans et al.*, 1989*a*]. A typical stress test consisted of setting a straddle packer within a distinct lithologic unit and pressurizing a 1.45-m interval until the rock fractured (Figure 3). Following initial breakdown, the induced fracture was reopened and extended through a series of pump/drain cycles. Estimated fracture radii were kept to about 4–7 m by limiting the volume of injected fluid to less than 100 L [*Evans and Engelder*, 1987]. Instantaneous shut-in pressure (ISIP) was measured downhole immediately after termination of each injection. Stabilized ISIP values obtained after several pump-drain cycles are interpreted as the total stress acting normal to the plane of the hydraulic fracture. Depending on the orientation of the hydraulic fracture, ISIP data measure either the vertical stress S_v or least horizontal stress S_h. The maximum horizontal stress is S_H. Figure 4 shows the magnitudes of the three principal stresses (S_H, S_h, S_v) measured in the Wilkins well including the two estimates of S_H discussed by *Evans et al.* [1989*a*]. The highest of the two was estimated from the breakdown pressure, the lowest from the reopening pressure. These data are listed in Table 3.

The Wilkins stress profile may be divided into three distinct stress zones: an upper zone, a transitional zone, and a lower zone (Figure 4). ISIPs in the upper zone lie close to the anticipated vertical stress and most likely reflect hori-

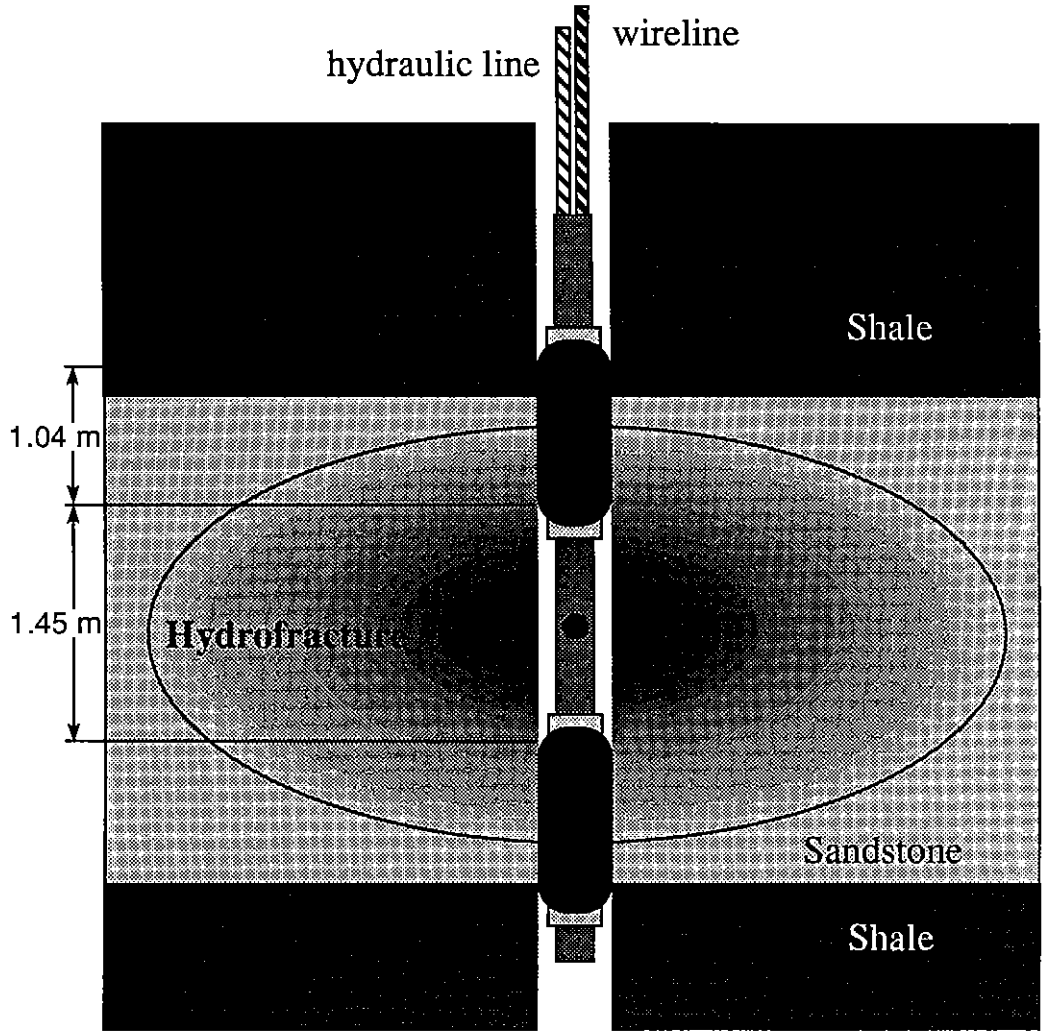

Fig. 3. Straddle packer tool used to conduct hydraulic fracture stress measurements (not to scale) showing stratified rocks targeted for stress measurements, the induced fracture plus dimensions of the packer seal (1.04 m), and the straddle interval (1.45 m). Borehole images are used to locate the tool within a targeted bed and small fluid volumes (10–100 L) are pumped to keep the hydraulic fracture within that bed.

zontal fracture growth where the horizontal stress level exceeds the vertical stress [*Evans et al.*, 1989*a*; *Evans and Engelder*, 1989]. For the purpose of discussion we simply say that these measurements are clipped at the value of the vertical stress. Stress data from the upper zone are of limited importance to this paper because they provide only lower bounds to the true value of the horizontal stresses and give us no information about the dependance of stress on lithology. ISIP data from the upper zone provide a good estimate of the vertical stress needed in subsequent analyses. ISIPs in transition zone shales decrease with increasing depth, whereas the ISIPs in the "sands" remain clipped at the value of the vertical stress. The lower regime is characterized by ISIPs which are substantially less than lithostatic. One exception is test 12 in the Tully Limestone where the ISIP again appears to be clipped at the vertical stress value (Figure 4). Principal and derived logs from the transition and lower zones are shown in Figures 5 and 6, respectively.

Geophysical Characterization of Stress Test Intervals

Many of the beds targeted for stress measurements were only a few meters thick. So, the log data had to be carefully depth matched to the stress measurement locations before we could characterize the physical properties of stress tested intervals. A depth match to better than 30 cm was achieved by determining the depths of common features observed in borehole images acquired using two different televiewers, one run on the wire line used to make stress measurements and the other run on the wire line used to acquire the geophysical log data. A depth shift curve was generated by plotting the apparent depth difference of a feature, such as a distinctive bedding plane, identified on both televiewer images, against the nominal depth of one of the logging cables. We observed depth shifts ranging between 0 and 2 m. We applied a depth correction to the data at each test location because the larger shifts are comparable to the thickness of some target beds and to the size of our hydraulic fractures. Once all the data were depth corrected, we computed arithmetic means of the geophysical parameters over a vertical distance which varied with each stress test. This distance was estimated from the height of the hydraulic fractures measured from digital televiewer images using methods described by *Plumb and Luthi* [1989]. When hydraulic fractures were not imaged clearly, we averaged over

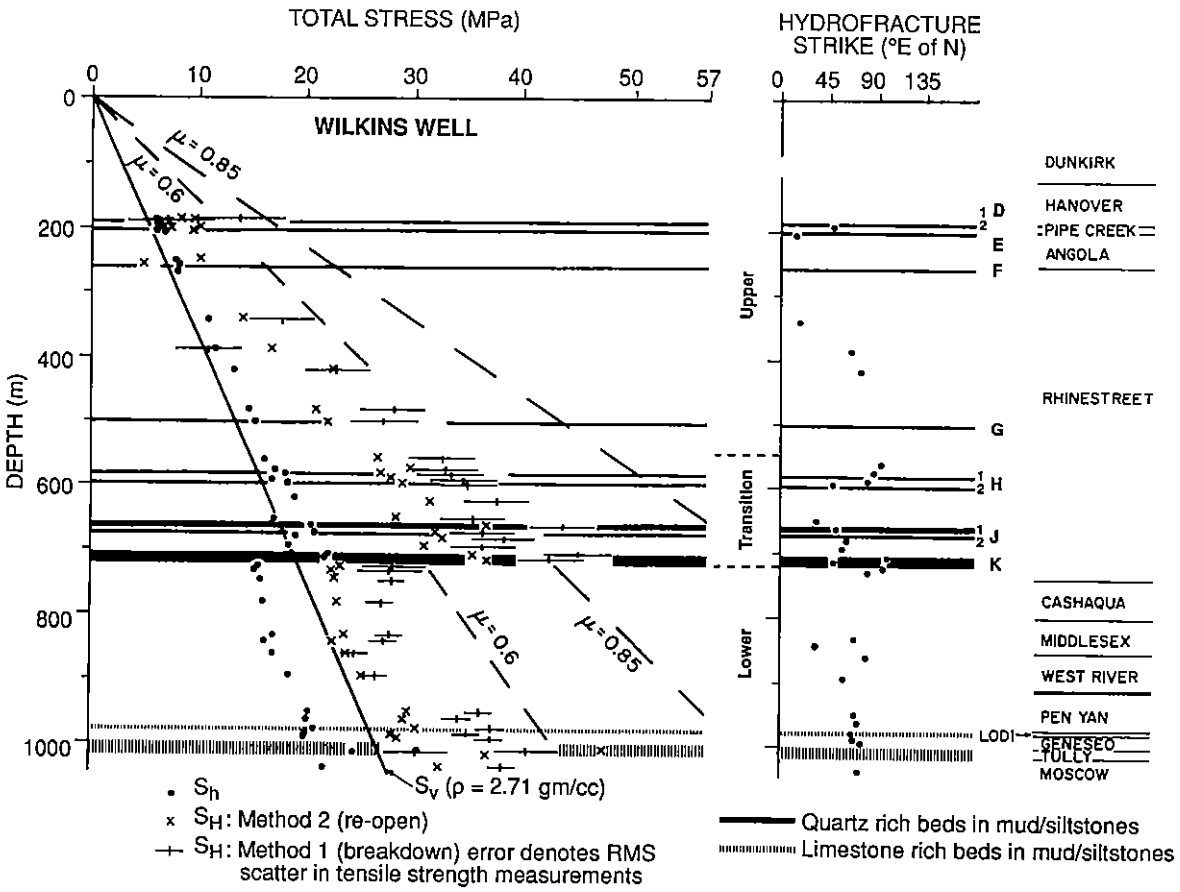

Fig. 4. Stress profile obtained in the Wilkins well showing key lithologies and the three principal stresses: S_v, S_h, and S_H. Two estimates of S_H are shown ${}^1S_H$ (method 1) and ${}^2S_H$ (method 2). ${}^1S_H$ is computed using the conventional breakdown equation and incorporating statistical data on the tensile strength of Devonian shales. ${}^2S_H$ is computed from the fracture reopening method. Dashed lines denote the S_H thresholds for cohesionless Coulomb failure for two internal friction angles assuming hydrostatic pore pressure. The least principal stress is taken as S_v above the K sand and S_h below. Three stress zones, the strike of hydraulic fractures and formation names are shown to the right [after *Evans et al.*, 1989*a*]. Notice the abrupt decrease in stress magnitudes at the base of the K sand, depth 720 m.

the straddle interval height of 1.45 m. Averaged physical properties of the stress test intervals are given in Table 3. The geophysical characteristics of each stress test interval are described below.

Geophysical logs effectively distinguish all lithologic units selected for stress testing. A plot of P_e versus K distinguishes limestones and "sands", plus the three shale groups: transition zone shales, lower zone grey shales, and lower zone black shales (Figure 7). Limestones have higher P_e and lower K than all of the other lithologies. The P_e for the Tully limestone (test 12) plots close to the value appropriate for calcite. In the transition zone, "sands" have lower P_e and lower K than shales. Potassium concentration in grey shales is similar to black shales but black shales have a lower P_e. The dominant clay type in all shales appears to be illite rather than chlorite. A greater P_e detected in transition shales is consistent with a bulk composition which may be greater in iron or chlorite (Table 2). Black shales are distinguished from transition zone shales in a plot of uranium concentration versus bulk density (Figure 8). Grey shale and transition "sands" have similar densities and U concentrations. The high U and lower bulk density for black shales is consistent with the observation that these rocks are highest in organic content [*Van Tyne*, 1982]. Bulk densities of "sands" and grey shales are greater than that of quartz or calcite indicating the presence of higher density minerals possibly feldspar, chlorite, or pyrite (Table 2). Transition zone shales plot well above the bulk density for limestone but appear similar to two grey shales (tests 18 and 37) and three "sands" (tests 38, 26, and 29). A neutron porosity greater than 20% distinguishes all shales from limestone and most "sands" (Figure 9). The highest neutron porosity is recorded in transition zone shales. Neutron porosity values are similar for grey and black shales. We interpret neutron porosity as a measure of hydroxyl content associated with clay-bound water in the shales. Based on potassium concentration and neutron porosity, black shales would appear to have clay contents similar to the other shales. However, resistivity of black shales is high in comparison with all other shales (Figure 10). It may be that organic material suppresses the surface conduction mechanism in these black shales. The lower-density and higher-U concentration of black shales suggests that organic material substitutes for some high-density, high-P_e mineral present in the other shales (Figures 7 and 8). In general, physical data suggest that the fractional volume of clay and hence its role as a load-bearing component at all stress test intervals increases with increased ϕ_n, increased potassium concentration, and

TABLE 3. Description of

Test Interval Description			Stress Magnitudes									
Test	Depth, m	Lithology*	S_h, MPa	${}^1S_H$, MPa	${}^2S_H$, MPa	$\langle S_H \rangle$, MPa	S_v, MPa	S_v^*, MPa	P_p, MPa	R_h	DTc, μs/ft	DTs, μs/ft
39	560.5	M.S.	16.05	32.65	26.45	29.55	14.95	17.07	5.90	0.940	73	142
14	579.0	M.S.	17.20	33.00	29.70	31.35	15.44	17.62	6.09	0.976	72	137
10	582.5	S.Sil.S. (H-1 sand)	18.20	33.40	27.00	30.20	15.53	17.73	6.13	1.027	66	113
24	592.5	M.S.	16.50	34.50	27.97	31.23	15.79	18.03	6.23	0.915	74	144
25	597.4	Sil.S. (H-2 sand)	18.30	32.35	28.90	30.63	15.92	18.18	6.28	1.007	67	118
38	621.8	Sil.M.S.	18.35	37.55	31.55	34.55	16.57	18.91	6.54	0.970	70	135
26	652.2	S.Sil.S.	17.00	35.40	28.25	31.83	17.37	19.82	6.86	0.858	69	127
27	662.5	S.Sil.S. (J-1 sand)	20.60	43.80	36.70	40.25	17.65	20.13	6.97	1.023	66	110
28	674.0	S.Sil.S. (J-2 sand)	20.60	36.30	32.15	34.23	17.95	20.47	7.09	1.006	66	110
29	680.0	Sil.S.	19.10	38.30	32.70	35.50	18.12	20.65	7.15	0.925	69	126
6	692.0	M.S.	18.50	36.50	31.10	33.80	18.44	21.01	7.28	0.880	73	140
31	707.5	S.Sil.S. (K sand)	21.95	45.10	35.50	40.30	18.84	21.48	7.44	1.022	66	118
15	712.5	S.Sil.S. (K sand)	21.85	42.60	37.05	39.83	18.98	21.63	7.50	1.010	66	119
16	724.0	Sil.M.S. (gry sh)	15.60	28.20	23.30	25.75	19.30	21.97	7.62	0.710	78	140
17	729.0	Sil.M.S. (gry sh)	15.40	27.75	22.55	25.15	19.42	22.12	7.67	0.696	78	137
18	747.0	Sil.S. (gry sh)	15.95	27.95	22.80	25.38	19.90	22.66	7.86	0.704	69	123
37	778.5	Sil.M.S. (gry sh)	16.05	26.95	22.85	24.90	20.72	23.61	8.19	0.680	70	130
19	832.5	Sil.M.S. (blk sh)	17.00	27.80	23.65	25.73	22.19	25.23	8.76	0.674	80	137
32	840.0	Sil.M.S. (blk sh)	16.25	27.20	22.70	24.95	22.37	25.45	8.84	0.638	83	136
33	860.5	Sil.M.S. (gry sh)	17.05	24.50	23.95	24.23	22.95	26.07	9.05	0.654	73	127
9	889.5	Sil.S. (gry sh)	18.50	26.45	25.45	25.95	23.70	26.94	9.36	0.687	69	118
34	951.0	Sil.M.S. (blk sh)	20.20	36.25	29.70	36.98	25.32	28.78	10.00	0.702	78	128
35	960.5	M.S. (blk sh)	20.00	34.35	29.20	31.78	25.59	29.07	10.10	0.688	81	132
36	977.6	L.S.	20.85	37.40	30.40	33.90	26.03	29.58	10.28	0.702	73	125
7	985.5	M.S. (blk sh)	19.90	35.20	28.20	31.70	26.16	29.82	10.37	0.667	89	180
8	991.2	M.S. (blk sh)	19.70	37.30	28.75	33.03	26.39	29.99	10.43	0.657	87	177
12	1009.5	L.S.	30.60	40.65	47.60	44.13	26.88	30.54	10.62	1.002	49	93
11	1013.5	L.S.	24.45	30.45	36.95	33.70	26.98	30.66	10.66	0.797	70	123

1 μs/ft = 3.2808 μs/m.

*Definition of lithology in terms of log responses after *Evans et al.* [1989*a*]: S.S., quartzitic sandstone, low γ (80 API), $\phi_n \leq \phi_d$; S.Sil.S., sandy siltstone; Sil.S., siltstone, moderate γ (100–120 API), $\phi_n \approx$ 15–20%, $\rho_b \approx 2.7$; Sil.M.S., silty mudstone; M.S., mudstone, high γ (<140 API), $\phi_n > 20\%$, $\rho_b \approx 2.7$.

decreased resistivity. Although it would appear from the preceding lithologic descriptions that P_e, resistivity, neutron porosity, and potassium concentration provide a qualitatively similar description of clay content, we show in the next section that stress is not always correlated to the same clay indicators. The differences appear when the data are divided into lithologic subgroups. We suggest that the correlation of stress with different clay indicators could reflect differences in the microstructure of the rocks.

Stress Magnitude–Geophysical Property Analysis

Having determined the state of stress and the average geophysical properties in each stress test interval, we can explore the possible mechanisms for generating the observed stress contrasts. In previous papers we have considered stresses resulting from horizontal tectonic strain, stresses, limited by rock shear strength and stresses resulting from paleo-overpressure drainage [*Plumb et al.*, 1987, *Evans et al.*, 1989*a*, *b*]. We will now show that mechanisms proposed to explain the stress contrasts in the Wilkins well, based upon core data from NY1, are compatible with geophysical data obtained at the well site. In particular, we show that the least horizontal stress S_h is greatest in the rocks with the highest Young's modulus and lowest clay content, both essential characteristics of a compressed-state stress profile.

Following are definitions of stress components used in the subsequent data analysis. The vertical stress is S_v; the maximum and minimum horizontal stresses are S_H and S_h, respectively. The average maximum horizontal stress $\langle S_H \rangle$ is the arithmetic mean of the two estimates of S_H shown in Figure 4: ${}^1S_H$ is computed using breakdown pressure together with statistical data on tensile strength of Devonian shales and ${}^2S_H$ is computed from fracture reopening pressure [*Evans et al.*, 1989*a*]. The vertical stress at depth h is computed as the total weight of the overburden

$$S_v = g \int_0^h \rho(z)\, dz \tag{1}$$

where $\rho(z)$ is the bulk density measured by the density log sampled every 15.2 cm of depth. ISIP data from the upper zone and one measurement in the Tully Limestone suggest that the vertical stress is about 10% greater than the overburden computed by equation (1). *Evans and Engelder* [1989] attributed this difference to the effect of topography in the study area. A linear regression of these ISIP data gives the following estimate of the vertical stress

$$S_v^* = 0.3z + 0.254. \tag{2}$$

Both estimates of S_v are given in Table 3 and both estimates have been included in the data analysis (Table 4).

Maximum shear stresses are computed as

$$\tau_{Hh} = \tfrac{1}{2}|S_H - S_h|$$
$$\tau_{Hv} = \tfrac{1}{2}|S_H - S_v| \tag{3}$$
$$\tau_{hv} = \tfrac{1}{2}|S_h - S_v|.$$

Shear stress components τ_{Hh} and τ_{Hv} have been computed using ${}^1S_H$, ${}^2S_H$, and $\langle S_H \rangle$. Stress components τ_{vh} and τ_{vH}

Each Stress Test Interval

Geophysical Properties													
V_p/V_s	K_b, GPa	G, GPa	E, GPa	ν	ρ_b, g/cm^2	P_e, b/el	ϕ_d	ϕ_n	CGR API	K, %	U, ppm	Th, ppm	log (R_a), log (Ω m)
1.95	30.52	12.69	33.38	0.32	2.75	3.76	0.00	0.27	132	3.4	2.28	17.13	1.69
1.90	30.93	13.52	35.38	0.31	2.73	3.74	0.01	0.28	124	3.9	2.64	15.43	1.70
1.71	31.64	19.38	42.28	0.25	2.67	3.25	0.05	0.17	96	2.7	2.33	13.38	1.98
1.95	28.98	12.14	32.00	0.32	2.73	3.81	0.01	0.28	121	3.9	3.22	14.52	1.67
1.76	32.53	17.86	45.31	0.27	2.70	3.40	0.03	0.20	111	3.1	1.50	15.50	1.99
1.93	32.69	13.93	36.55	0.31	2.73	3.55	0.01	0.24	122	3.7	2.37	15.80	1.80
1.84	31.49	16.48	41.93	0.28	2.74	3.78	0.01	0.24	118	3.6	3.41	15.11	1.77
1.67	28.38	20.48	49.52	0.21	2.66	3.13	0.05	0.15	91	2.0	2.97	14.74	2.06
1.67	28.86	20.34	49.31	0.21	2.67	3.24	0.05	0.18	100	2.7	3.18	14.22	1.98
1.83	32.53	16.00	41.17	0.29	2.73	3.62	0.01	0.25	117	3.6	2.86	15.21	1.77
1.92	30.65	12.97	34.07	0.32	2.74	3.92	0.01	0.28	132	4.2	2.23	16.41	1.65
1.79	32.69	18.07	45.72	0.27	2.70	3.31	0.03	0.20	113	3.3	1.78	15.00	1.89
1.80	33.32	17.72	45.10	0.28	2.71	3.29	0.03	0.21	110	2.9	2.26	15.89	1.92
1.79	23.38	12.97	32.83	0.27	2.72	3.55	0.02	0.26	126	4.0	2.08	15.51	1.69
1.76	23.30	13.17	33.31	0.26	2.69	3.75	0.04	0.27	130	4.2	2.69	15.52	1.77
1.78	32.38	16.76	42.90	0.28	2.73	3.48	0.01	0.24	117	3.7	2.26	14.69	1.76
1.86	31.21	15.10	39.03	0.29	2.74	3.51	0.03	0.26	123	4.2	2.80	14.13	1.75
1.71	20.53	13.10	32.41	0.24	2.65	3.32	0.06	0.25	117	3.8	4.08	14.09	1.83
1.64	17.96	13.03	31.52	0.21	2.61	3.12	0.08	0.26	118	3.8	3.96	14.51	1.91
1.74	27.05	15.45	38.97	0.26	2.71	3.61	0.02	0.24	118	3.8	2.51	14.34	1.71
1.71	28.15	17.72	44.00	0.24	2.69	3.34	0.04	0.21	108	3.4	2.77	13.44	1.87
1.64	20.05	15.03	36.07	0.20	2.65	3.24	0.06	0.25	119	3.5	4.78	15.75	2.07
1.63	18.69	13.93	33.45	0.20	2.64	3.33	0.07	0.26	124	4.0	3.35	14.95	2.09
1.71	24.20	15.79	38.83	0.23	2.63	3.94	0.08	0.17	70	2.4	3.70	7.95	2.26
2.02	20.05	7.24	19.38	0.34	2.53	3.34	0.13	0.26	110	3.9	11.12	11.80	2.29
2.03	21.16	7.59	20.28	0.34	2.57	3.18	0.11	0.26	115	3.9	8.14	13.23	2.33
1.90	68.28	29.03	76.21	0.31	2.73	4.73	0.01	0.03	28	0.7	0.74	3.94	3.24
1.76	29.22	16.62	41.93	0.26	2.69	4.23	0.04	0.15					1.89

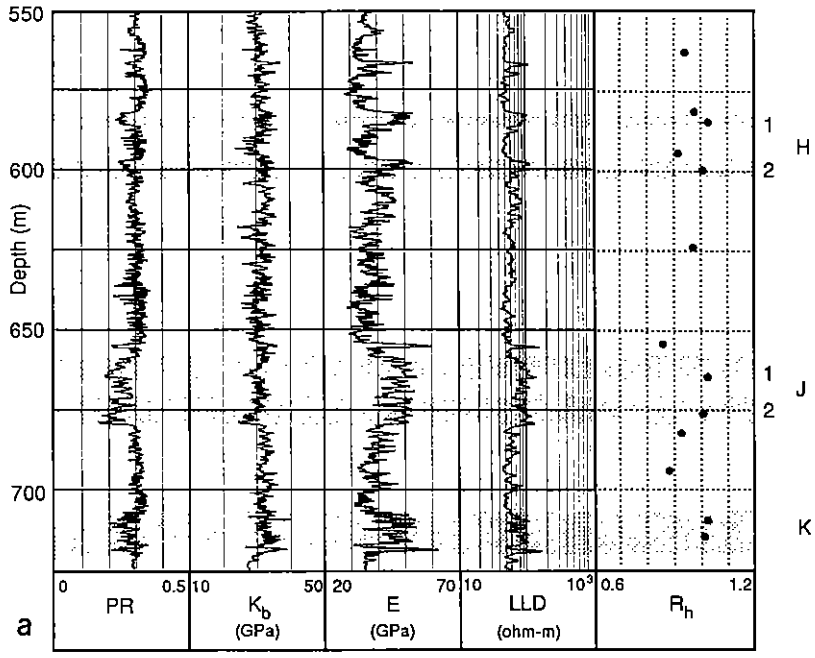

Fig. 5. Principal and derived log data for the transition zone showing the location of "sands" (H–K) and stress ratio R_h (equation (4)): (*a*) Poisson's ratio (PR), bulk modulus (K_b), Young's modulus (E), resistivity (LLd); (*b*) compressional wave velocity (V_p), shear wave velocity (V_s), bulk density (ρ_b), bulk porosity (ϕ_d), neutron porosity (ϕ_n); (*c*) spectral gamma ray (SGR), uranium concentration (Uran), thorium concentration (Thor), potassium concentration (Pota) and photoelectric absorption factor (P_e). Notice that R_h is highest in the "sands" and lowest in the shales (cf. Table 1 for log responses).

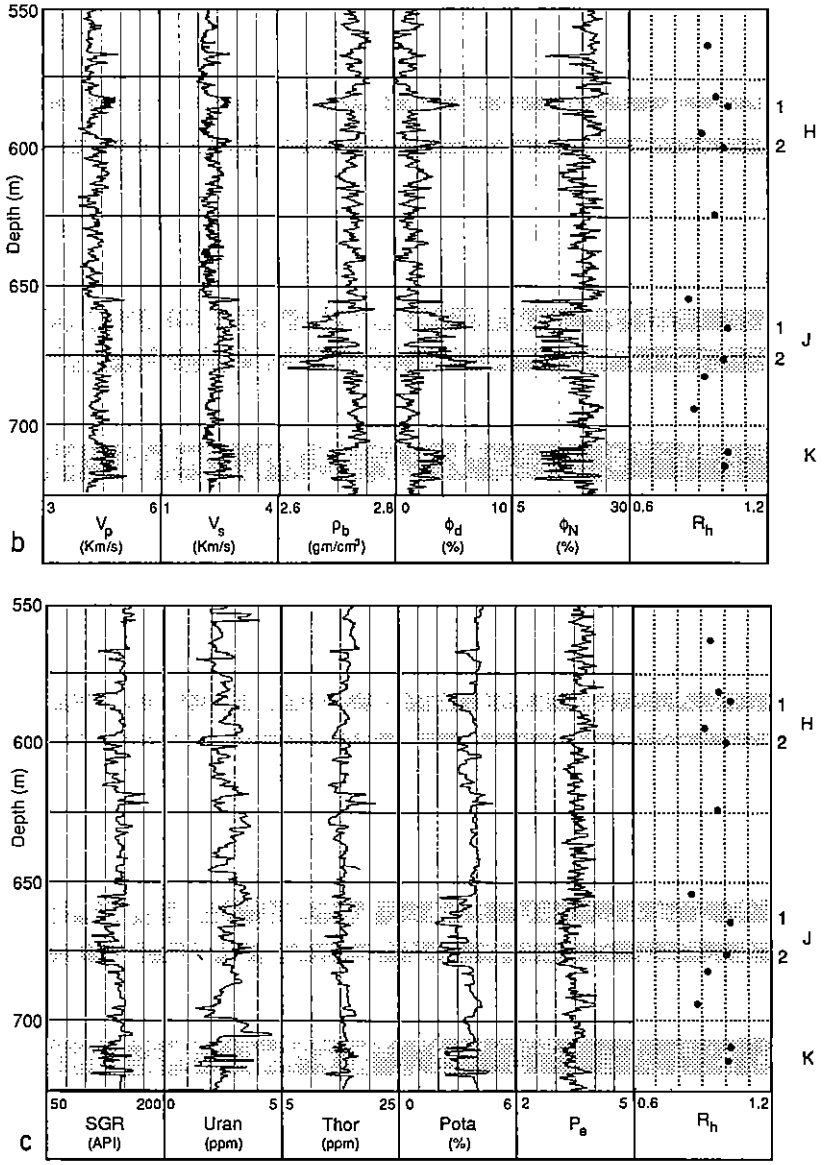

Fig. 5. (continued)

have been computed using S_v^*. There are no estimates for shear stress in the transition zone "sands" where S_H or S_h are clipped at the value of S_v. Shear stress components are estimated for all tests in the lower zone except for the Tully Limestone test 12 where both S_H and S_h are unknown.

The ratio of the minimum horizontal to vertical total stress,

$$R_h = S_h/S_v, \tag{4}$$

is a convenient normalization which emphasizes lithologic stress contrasts and provides a measure of the departure from lithostatic stress.

Multiple linear regression analysis was used on data in Table 3 to help identify relationships among stress parameters and interval-averaged physical properties. The result of the regression analysis is a correlation matrix giving the correlation coefficients r between all pairs of variables. Correlation coefficients may range from -1 to 1. An $r = 1$ indicates a perfect positive correlation, $r = -1$ indicates a perfect negative correlation, and $r = 0$ indicates no correlation. The correlation matrix provides an means for identifying trends in the data. We do not estimate the statistical significance of these results since there are relatively few data points and since some correlations are strongly influenced by two limestone tests (tests 11 and 12). However, highly correlated factors place constraints on admissible geophysical models for the observed lithology dependent stress variations. From a few poorly correlated factors we were able to identify the major physical differences between rocks of the transition and lower zones.

Correlation matrices were computed for seven different data groupings, each chosen to investigate a particular aspect of the Wilkins stress profile (Figure 11). The data groups are all lithologies (shales, "sands", limestones) in the transition and lower zones (TZ + LZ: All); shales in both zones (TZ + LZ: Shales); shales and "sands" in the transition zone (TZ: All); shales in the transition zone (TZ: Shales); shales and limestones in the lower zone (LZ: All); lower zone shales (LZ: Shales); and shales and limestones from the base of the lower zone (Base LZ: All).

The "TZ + LZ: All" group is best suited to search for

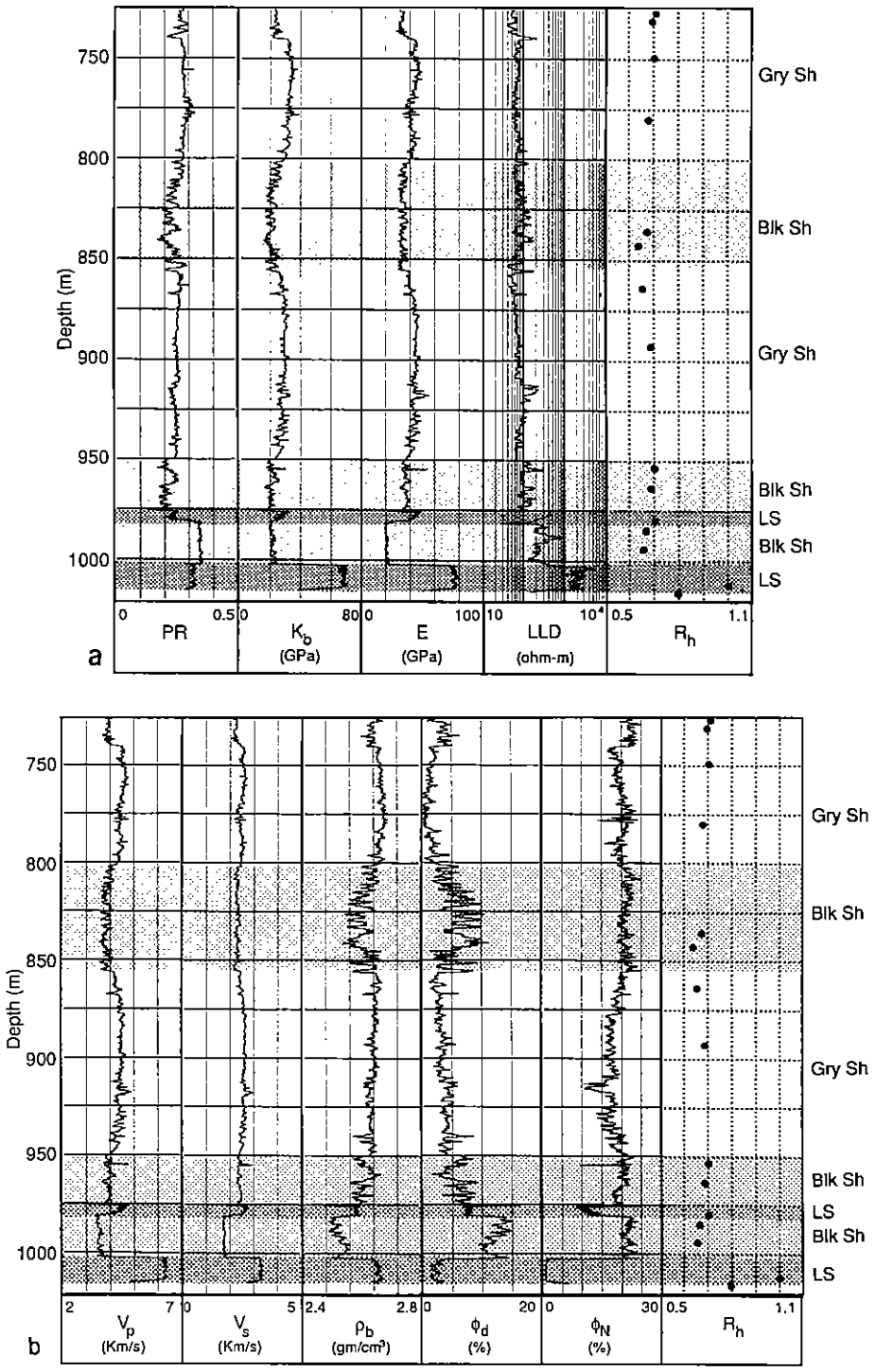

Fig. 6. Principal and derived log data for the lower zone showing the locations of "black" shales (Blk Sh), "grey" shales (Gry Sh), limestones (LS) and stress ratio R_h (equation (4)): (*a*) Poisson's ratio (PR), bulk modulus (K_b), Young's modulus (E), resistivity (LLd); (*b*) compressional wave velocity (V_p), shear wave velocity (V_s), bulk density (ρ_b), bulk porosity (ϕ_d), neutron porosity (ϕ_n); (*c*) spectral gamma ray (SGR), uranium concentration (Uran), thorium concentration (Thor), potassium concentration (Pota) and photoelectric absorption factor (P_e). Notice that R_h is highest in the limestones and lowest in the black shales (cf. Table 1 for log responses).

correlations between rock properties and the major stress decrease at the base of the K sand. The "TZ: All" and "LZ: All" groups are used to search for correlations between physical properties and the stress variations within each zone. Three shale groups were analyzed for physical properties which might explain small stress variations among shales. The "Base LZ: All" group focuses on a sequence of black shales and limestones which is characterized by large contrasts in physical properties and stress magnitudes.

Overall, the strongest correlations are observed where stress contrasts and the physical property contrasts are both large. These large contrasts are most commonly observed

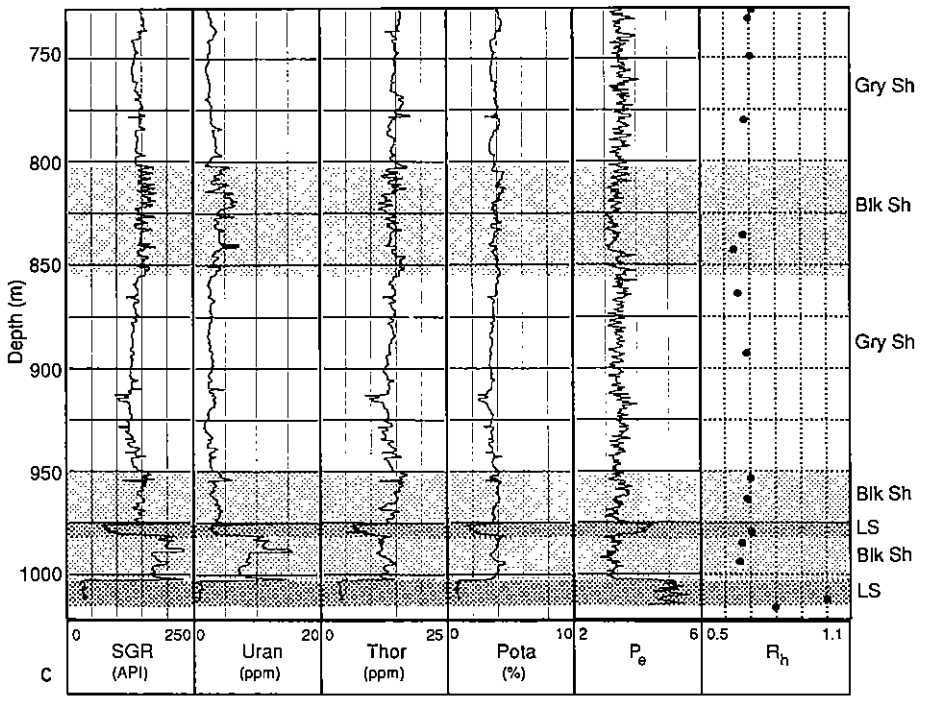

Fig. 6. (continued)

between shales and sandstone or shales and limestone. Large stress contrasts are not common among shales of a given stress zone, and there are no significant correlations between physical properties of shales and stress magnitudes within the transition zone or the lower zone. However, correlations are observed for shales which span the stress discontinuity (TZ + LZ: Shales). Table 4 summarizes five correlation matrices showing all the physically significant correlations observed for each data group. None of the correlations are driven by correlation of either parameter with depth and no significant correlations were found in the two remaining shale data groups.

Transition-lower zone all. In this data group we analyze all measurements on either side of the stress decrease at the base of the K sand. This data group represents the broadest range of stress magnitudes and physical properties in this study. S_h is the only stress component significantly correlated to formation properties across the two zones (Table 4). The strongest correlations with S_h are resistivity log (R_a), neutron porosity ϕ_n, potassium content K, and corrected gamma ray CGR. The correlations with ϕ_n and log (R_a) are shown in

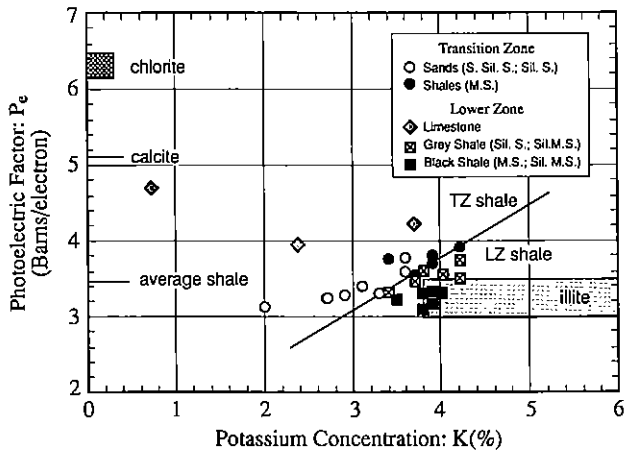

Fig. 7. Geophysical signature of stress test intervals as shown by a plot of photoelectric factor (P_e) versus potassium concentration (K). Shown for reference are the approximate fields for chlorite and illite plus the P_e of calcite and average shale [after *Ellis*, 1987]. Limestones are distinguished from shales and "sands"; diagonal line separates transition zone "sands" and shales from lower zone grey shales and black shales; shale composition appears to be rich in illite.

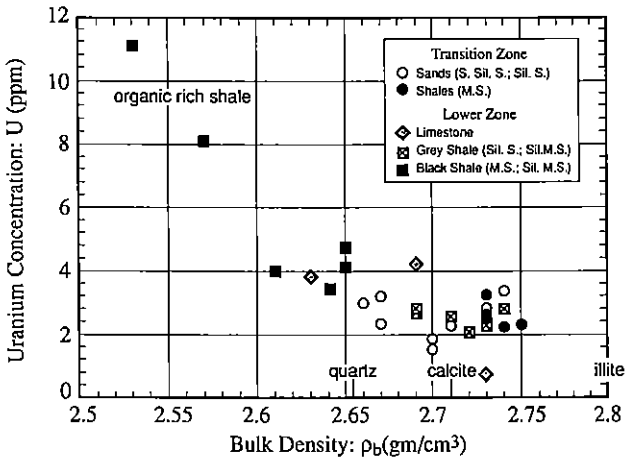

Fig. 8. Geophysical signature of stress test intervals as shown by a plot of uranium concentration (U) versus bulk density (ρ_b). The ρ_b of quartz, calcite, and illite are shown for reference. Black shales have lower density and higher U than other rocks particularly tests 7 and 8 (upper left). Their low density and high U is attributed to high organic content.

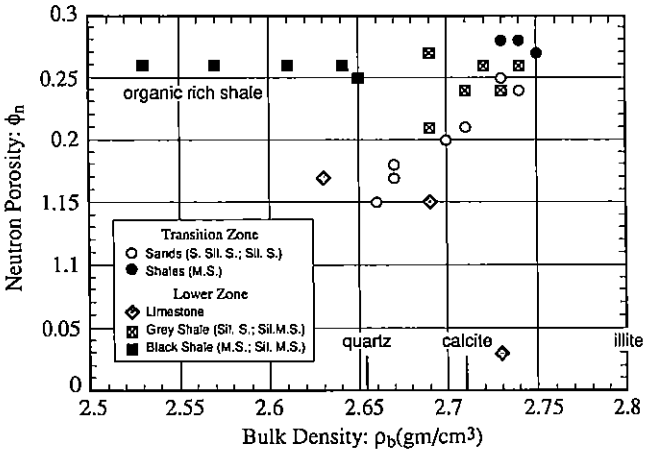

Fig. 9. Geophysical signature of stress test intervals as shown by a plot of neutron porosity (ϕ_n) versus bulk density (ρ_b). The ρ_b of quartz, calcite, and illite are shown for reference. Bulk density increases with increasing neutron porosity except for organic-rich black shales (upper left) and the Tully Limestone (lower right).

Figure 12. Collectively, these correlations indicate that greater stress magnitude is associated with lower clay content.

Transition-lower zone shales. This data group contains the most well-constrained stress magnitude data spanning the two zones. Correlations from this data set provide the strongest physical property constraints on the interpretation of the stress decrease below the K sand. Weak correlations are indicated between bulk porosity R_h, bulk modulus K_b, and photoelectric absorption factor P_e (Table 4). These correlations reflect the macroscopic porosity and compositional differences between the transition and lower zone shales. The negative correlation coefficients for porosity and bulk modulus are consistent with the hypothesis that shales in the lower zone are undercompacted relative to shales in the transition zone [*Engelder and Oertel*, 1985; *Evans et al.*, 1989*a*].

Transition zone all. Examination of the logs in Figure 5 shows that higher values of R_h are found in rocks with greater Young's modulus and lower clay content. This general trend is seen in the correlation matrix, but it is not statistically robust because the magnitudes of S_H and S_h are not precisely known in the "sands" (Table 4). Stress ratio R_h is greatest in the low-P_e, low-ϕ_n "sands" where porosity and elastic moduli E and G are high. Figure 13 illustrates two characteristics of the compressed-state stress profile: a higher R_h in "sands" with low-P_e, and high-E compared to shales with lower E and higher P_e.

Lower zone all. Elastic moduli logs clearly show that stiffer rocks are under greater stress, particularly those at the base of the zone (Figure 6). R_h is positively correlated with log (R_a), K_b, E, and G and negatively correlated with ϕ_n (Table 4). Figure 14 shows the variation in R_h with E and ϕ_n. Limestones have higher stress, higher Young's modulus, and lower neutron porosity than shales.

Base of the lower zone all. Stress magnitudes and rock properties are strongly correlated in this zone of well-defined lithologic and stress contrasts (Table 4). R_h, S_h, and S_H are positively correlated to P_e, elastic stiffness moduli K_b, E, G, electrical resistivity log (R_a), and negatively correlated with clay indicators ϕ_n. Figure 15 shows higher R_h in intervals with higher E and lower ϕ_n. The inconsistent correlations between shear stress, bulk density, and elastic moduli simply reflect the lithology dependent variations of S_h and S_H and have nothing to do with micromechanical deformation mechanisms (Table 4). We will return to this point later.

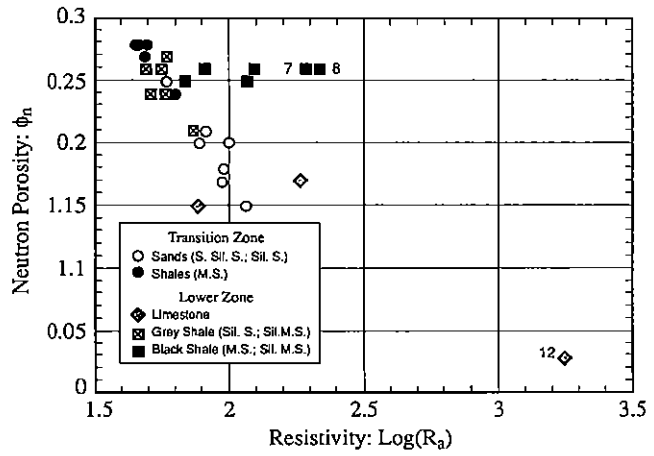

Fig. 10. Geophysical signature of stress test intervals as shown by a plot of neutron porosity (ϕ_n) versus electrical resistivity log (R_a). Resistivity increases as the neutron porosity (clay content) decreases except for the most organic rich black shales, tests 7 and 8, suggesting that number of interconnected clay particles or the amount of load-bearing clays decreases as resistivity increases. In black shales, organic material is substituted for high-density, high-P_e clays.

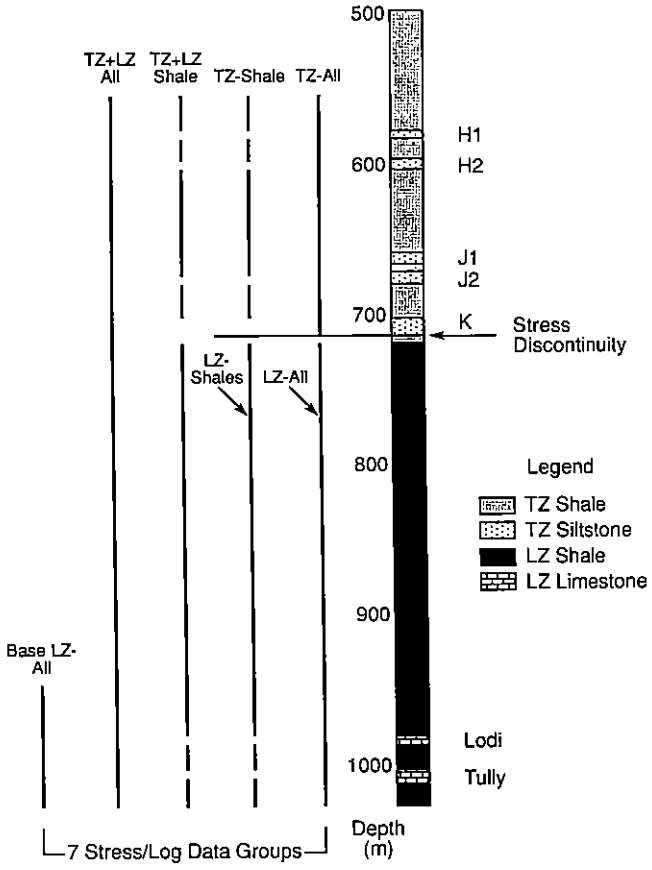

Fig. 11. Diagram showing the seven data groups used in the multiple regression analysis.

TABLE 4. Summary Correlation Matrices for Five Data Groupings Giving the Correlation Coefficients r Between Stress Parameters and the Log-Derived Geophysical Properties

	Data Group							
	TZ+LZ: All	TZ+LZ: Shale	TZ: All	LZ: All	Base LZ: All			
Stress parameter	S_h	R_h	R_n	R_h	R_h	τ_{Hh}	τ_{Hv}	τ_{hv}
Geophysical property								
log (R_a)	0.87			0.80	0.94			
ρ_b			−0.79			0.91		−0.87
ϕ_d		−0.65	0.80					0.87
ϕ_n	−0.81		−0.75	−0.91	−0.95			
K_b		0.70		0.93	0.99			
E			0.67	0.88	0.97	0.86		−0.96
G			0.67	0.85	0.94	0.85		−0.97
P_e		0.70	−0.89		0.92			
K	−0.80							
U						−0.90	0.89	
CGR	−0.83							

See Table 1 for a definition of the geophysical properties. No correlations are driven by a depth dependence of the parameters.

DISCUSSION

We have shown that the least horizontal principal stresses are correlated with physical properties of the rocks in the Wilkins well. Significant stress differences are greatest between major lithologies, such as limestone, siltstone, and shale, but smaller stress differences are found within a given lithology such as shale. The general trends are such that

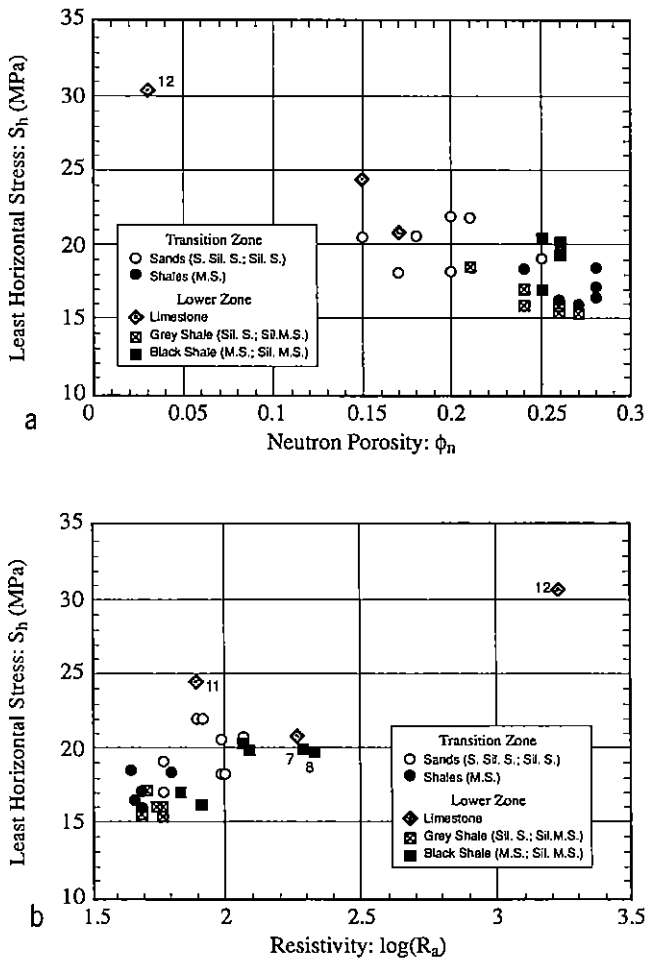

Fig. 12. Stress correlations in the transition-lower zone group (TZ + LZ: All): (*a*) least horizontal stress S_h versus neutron porosity ϕ_n, showing rocks with lower ϕ_n have higher stress; (*b*) S_h versus resistivity log (R_a), showing rocks with higher electrical resistivity have higher stress. Low-stress rocks with low resistivity and high ϕ_n have a high clay content.

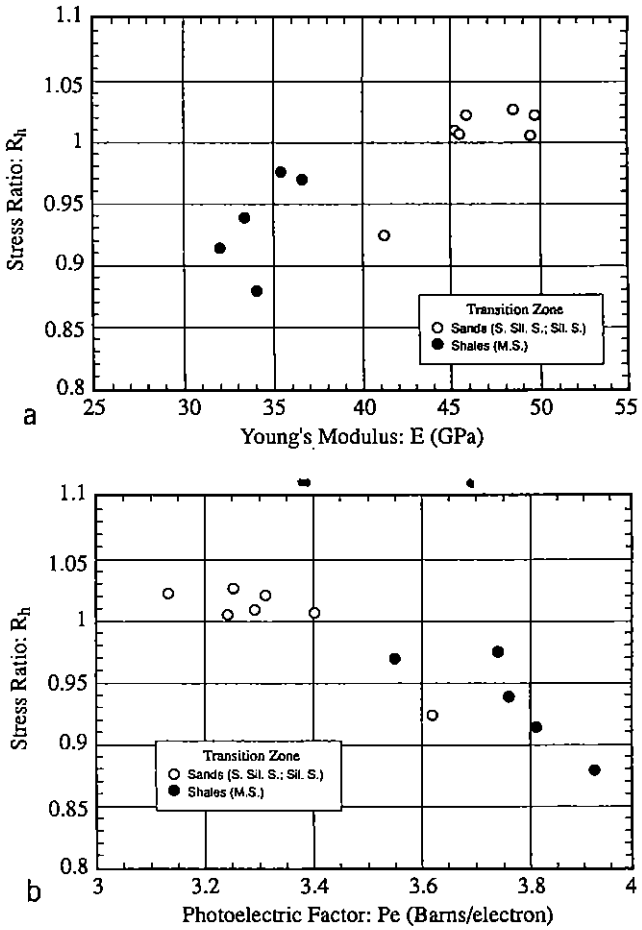

Fig. 13. Stress ratio correlations for "sands" and shales in the transition zone group (TZ: All): (*a*) stress ratio R_h (equation (4)) versus Young's modulus E, showing higher modulus and higher stress in "sands" compared to shales, R_h is a lower bound in "sands"; (*b*) R_h versus photoelectric factor P_e, showing shales with higher P_e and lower stress than "sands." Low-stress shales have higher P_e (more illite?) and lower E than high stress "sands."

stress magnitude variations are proportional to elastic stiffness, electrical resistivity, and P_e but inversely proportional to neutron porosity (Table 4). A compressed-state stress profile is clearly indicated by the correlation of high stress with high stiffness and low clay content. Correlation coefficients tended to be lower for data groups combining data from two stress zone than for individual zones. We would expect this if the mechanism responsible for the major stress decrease at the base of the K sand is different from that which accounts for the local bed-to-bed variations. For example, there is a clear correlation between stress magnitude and Young's modulus for each stress zone (e.g., Figure 13). This is strikingly evident in the profiles shown in Figures 5 and 6. Yet no significant correlation is indicated when the combined data (TZ + LZ: All) are considered. Rather we find that the combined data suggest a weak correlation between the least horizontal principal stress and neutron porosity and potassium content (Table 4 and Figure 12). This emphasizes the need for careful selection of data groupings for resolving physically relevant correlations. A further point of note is that high correlation coefficients often reflect the effects of one or two beds whose material property and stress level contrast strongly with the average. This is true

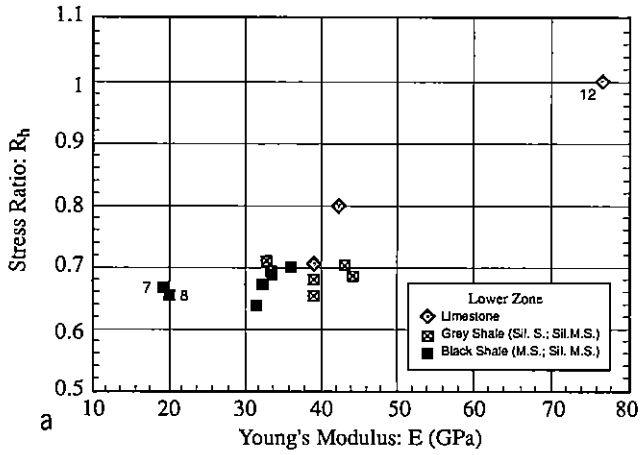

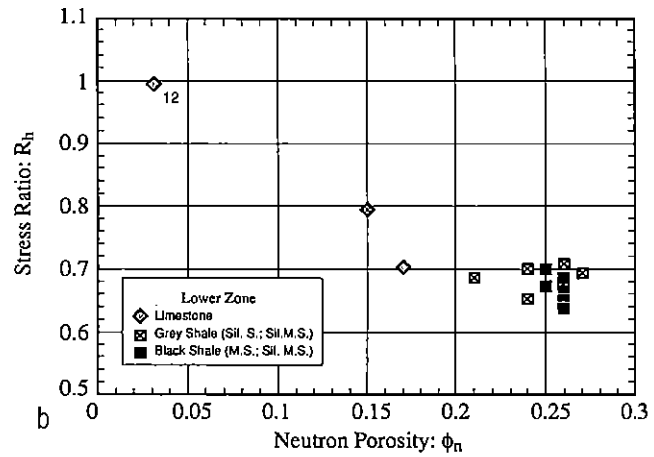

Fig. 14. Stress ratio correlations in the lower zone group (LZ: All): (*a*) stress ratio R_h versus Young's modulus E, showing higher modulus and higher stress in limestones compared to shales, R_h is a lower bound in the Tully Limestone test 12; tests 7 and 8 are organic rich black shales; (*b*) R_h versus neutron porosity ϕ_n, showing higher stress in rocks with lower ϕ_n. Shales have lower stress, lower E, and higher clay content than limestones.

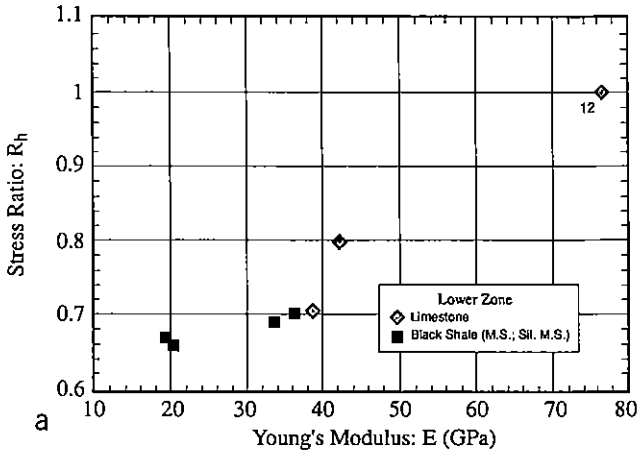

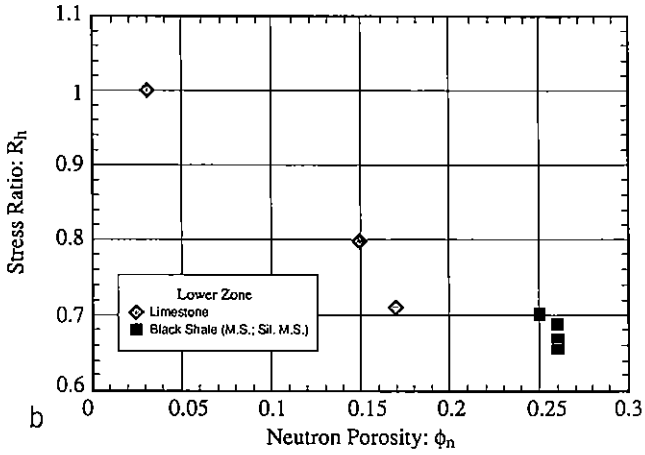

Fig. 15. Stress ratio correlations in the base lower zone group (Base LZ: All): (*a*) stress ratio R_h versus Young's modulus E, showing higher modulus and higher stress in limestones compared to black shales; R_h is a lower bound in the Tully Limestone test 12; (*b*) R_h versus neutron porosity ϕ_n, showing higher stress in rocks with lower ϕ_n. Correlations between stress and lithology are similar but stronger than those of Figure 14; low stress correlates with high clay content.

for the Tully Limestone data point (test 12) and accounts for the high correlation coefficients obtained for the lower zone data groups (Figures 12, 14, and 15). Although more uniform spatial sampling is desirable from a statistical viewpoint, it is unlikely to be realized in real geologic situations. Moreover, it is reasonable that data points obtained from beds whose physical properties deviate strongly from the average should exert the strongest influence on the correlation since, for our purposes, these beds provide the greatest signal to noise ratio. Nevertheless, correlation trends which are strongly influenced by the Tully Limestone data point (test 12) and the "sands" data points for the transition zone are only qualitative since we only have lower bound estimates of the stress ratio.

Microstructure Model

By exploring the physical significance of these correlations we provide a qualitative picture of the load-bearing framework of these strata: one that places constraints on deformation mechanisms and the boundary conditions affecting them. The neutron measurement is sensitive to the total hydroxyl content of the formation. Hydroxyls in low-

porosity Devonian shales are associated with clay minerals and to a lesser extent water in poorly connected pores. P_e is sensitive to the average atomic number of rock-forming elements and therefore is a measure of the rock frame composition. High P_e levels in clastic sedimentary rocks usually indicate increasing amounts of iron or calcite. Increased iron in Devonian shales could indicate increased amounts of illite, chlorite, pyrite, or siderite. The P_e level measured in shales and siltstones is consistent with the majority of clays being illite. P_e higher than 3.6 in shales could indicate increased amounts of chlorite or a calcite cement (Table 2). Near the base of the section, increased P_e is a response to calcite associated with the Lodi and Tully limestones. Of course, P_e does not uniquely determine the mineralogy: P_e variations among the shales can be modeled by different volumetric mixtures of the minerals mentioned above [*Ellis*, 1987].

Electrical resistivity was consistently correlated with stress magnitude. In shaly sands, electrical conductivity depends upon the conductivity of the pore fluids, the tortuosity of the pore space, and surface conductance between contacting clay minerals [*Sen*, 1987]. Surface conductance is due to counter ions that balance charge defects in the lattice of clay minerals. In well-consolidated shales, connected fluid-filled porosity is generally very low so that electrical conductivity is generally dominated by surface conductance effects among load-bearing clays. Increased resistivity of the shales should indicate decreased interconnectivity of clay minerals or, perhaps in the case of black shales, more organic matter. In contrast, increased resistivity in limestones is due to decreases in the amount of connected fluid-filled pores. Since the shear strength of rock is expected to increase as the porosity and the amount of load-bearing clay decrease, the observed increase in electrical resistivity is consistent with a decrease in clay content or porosity and an increase in shear strength.

Elastic wave velocities provide the most direct mechanical measurements of the load bearing rock frame. The shear modulus, Young's modulus, bulk modulus, and Poisson's ratio are determined using equations (A1)–(A4). To a first approximation, variations in modulus reflect variations in the composition of the load-bearing minerals such that moduli of shales and siltstones are dominated by the average moduli of the clays. Increasing elastic stiffness is assumed to be an indication of decreasing amounts of clay in the load-bearing frame where the decreased clay content is balanced by increases in the amount of quartz or carbonate. The assumption is corroborated here since we find a concomitant increase of the calculated elastic moduli with increased electrical resistivity and decreased neutron porosity. These physical characteristics are consistent with a rock frame having decreased amounts of load-bearing clays and greater shear strength. Figure 16 shows a microstructural model of stress tested strata inferred from geophysical logs indicating that shales have more load-bearing clay minerals than siltstones.

Nature of the Stress-Lithology Correlations

Are the observed correlations between stress and lithology the result of elastic deformation or a consequence of the critical shear strength of the various strata? *Evans et al.* [1989*a*] examined the hypothesis that the stress measured here is limited by the shear strength of the formations. By modeling shales of the lower zone as a cohesionless Coulomb material subjected to a maximum shear stress τ_{Hh}, *Evans et al.* [1989*a*] concluded that the shales are not close to shear failure for reasonable values of the coefficient of internal friction (μ = 0.6 to 0.85) (Figure 4). The coefficient of internal friction would have to be approximately, μ = 0.3, to match the stresses in these shales. Furthermore, correlations between physical properties and shear stress magnitudes do not support the critical shear strength hypothesis. If shear stresses are limited by rock shear strength, we only expect the maximum shear stresses to be correlated with factors controlling rock strength, and we expect shear stresses to increase as the amount of load-bearing clay decreases. The most reliable shear stress estimates are obtained in the lower zone where the maximum shear stress is either τ_{Hh} or τ_{hv}, depending on the location of the stress test. Only shear stresses computed using ${}^2S_H$ show any correlation to material properties. This, however, is not our preferred estimate of S_H [cf. *Evans et al.*, 1989*a*]. There were no significant correlations between clay indicators and τ_{hv} and only the uranium concentration U is correlated with τ_{Hh}. The correlation between τ_{hv} and U is physically reasonable since shear stress increases as the organic content decreases. Under the critical shear strength hypothesis, this observation suggests that organic content could be an important factor controlling shear strength of these shales. The positive correlation between τ_{Hv} and organic content (Table 4) is not meaningful under the critical strength hypothesis because the magnitude of τ_{Hv} is the lowest of the three shear stress components and organic content is high when shear stress is high. The lack of correlation with the other clay indicators and is also troublesome. Finally, apparently conflicting correlations between τ_{Hh}, τ_{hv}, and elastic moduli can be explained by principal stress variations that correlate with changes in elastic modulus. τ_{Hh} is positively correlated with elastic stiffness because S_H and S_h are positively correlated with stiffness. τ_{hv} is negatively correlated with stiffness because the difference between S_h and S_v decreases as stiffness increases.

An alternative model for the observed stress profile assumes the strata are subjected to a horizontal elastic strain. This model correctly predicts the observed sense and relative magnitude of lithologic stress contrasts among beds with different elastic moduli [*Plumb et al.*, 1987; *Evans et al.*, 1989*b*]. It predicts higher stresses in elastically stiffer lithologies, which, for the Wilkins well, corresponds to strata with smaller amounts of load-bearing clays. The horizontal strain model is consistent with the microstructural interpretation of the strata based on all the log responses correlated to stress magnitudes.

If a regional tectonic strain is responsible for lithologic stress contrasts measured in the Wilkins well, then we would expect to find a similar correlation in the nearby Auburn well. *Hickman et al.* [1985] conducted four open hole hydrofracture stress measurements to a depth of 1482 m at Auburn, New York (Figure 1). Stress was measured in a sandstone, two shaly sandstones and a shale, all of which are stratigraphically lower than sedimentary rocks encountered in the Wilkins well. To examine the tectonic strain hypothesis at Auburn, we computed Young's modulus and the stress ratio R_h at the nominal depth of the stress tests using S_v and geophysical log data reported by *Plumb and Singer*

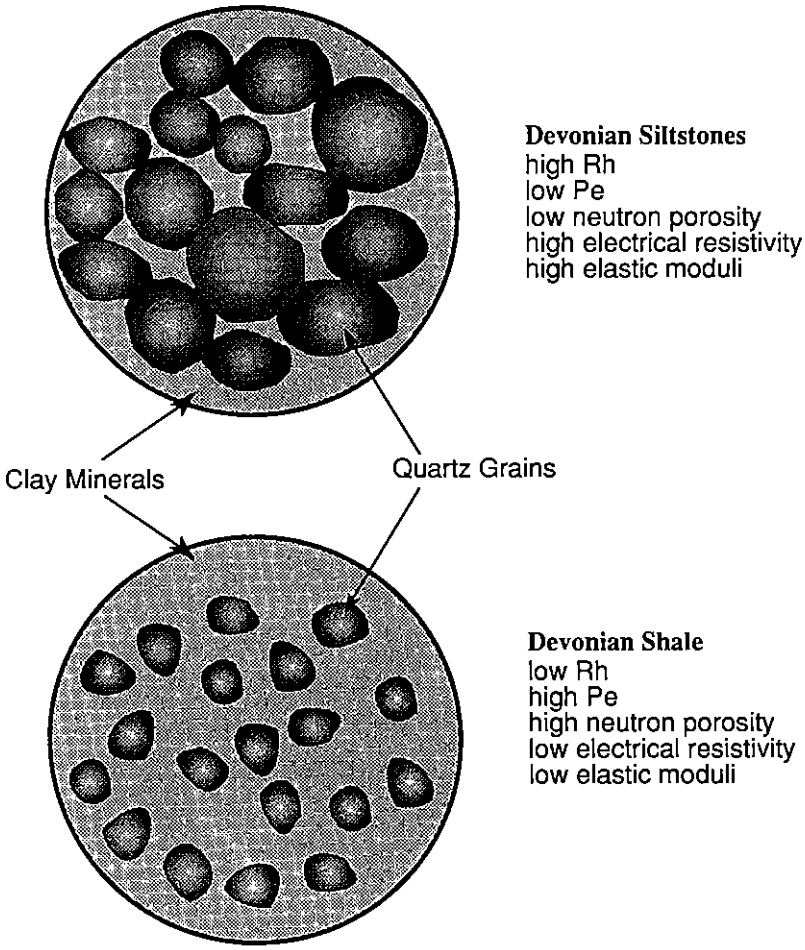

Fig. 16. Microstructure of siltstones (top) and shales (bottom) inferred from physical properties correlated with stress magnitudes. More of the load bearing minerals in high-stress siltstones are quartz grains giving the rock a high Young's modulus and high resistivity. Lower-stress shales have more clay minerals as indicated by their higher P_e and higher ϕ_n. Lower resistivity and lower Young's modulus are taken as an indication that more of the load applied to the rock is supported by interconnected clay particles.

[1983]. Figure 17 shows that R_h increases as Young's modulus increases. Notice that the stress ratio in shale is relatively low compared to the other rock types. This suggests that modulus and not apparent clay content controls the stress variations at Auburn. Results from the Auburn and Wilkins wells are consistent with the horizontal strain model.

Geophysical models for the origin of the lithologic stress contrasts observed in the Wilkins well have been extensively discussed elsewhere [*Evans and Engelder*, 1987; *Evans et al.*, 1989*b*; *Evans*, 1989]. *Evans et al.* [1989*b*] constrained their interpretations by regional geologic data as well as rock fabric and mechanical property measurements made on cores from NY1, a well located 20 km northwest of the Wilkins well (Figure 1). Core data corroborate initial log interpretations, showing that stress magnitudes were greater in elastically stiffer strata [*Plumb et al.*, 1987]. *Evans et al.* [1989*b*] concluded that the bed-to-bed stress contrasts were best explained by a uniform horizontal elastic strain. Addition information provided by geophysical logs in the Auburn and Wilkins data extends the apparent strain signature to include the entire Paleozoic section of New York State.

The stress decrease near the base of the K sand correlates with a regionally observed undercompaction of sediments below the Rhinestreet [*Engelder and Oertel*, 1985; *Evans et al.*, 1989*b*]. *Evans et al.* [1989*b*] argue that the magnitude of the stress decrease could be explained by a reduction of high pore pressure. If so, we expect higher-porosity rocks below the K sand. Figure 18 shows average porosity in shales from the stress test intervals of the transition and lower zones. Shales of the lower zone are indeed less consolidated than those in the upper zone in accord with regional compaction data. Consolidation appears to decrease slightly with depth in the lower zone. The stress decrease is manifested in the transition-lower zone composite data group as good correlations between S_h and neutron porosity, potassium concentration, corrected gamma ray, and electrical resistivity (Table 4). Neutron porosity and electrical resistivity correlations are associated with the compositional differences between "sands" of the transition zone and shales of the lower zone. The stress decrease at the base of the K sand is also reflected in the transition–lower zone shale data group as a weak but physically significant correlation among R_h, ϕ_d, K_b, and P_e (Table 4). These correlations are consistent with the observation that shales in the lower zone are compositionally different and undercompacted relative to shales in the transition zone.

Regional implications. Regional stress studies of the

Appalachian Plateau show that the contemporary stress field affecting the entire Paleozoic section and basement contains a component of ENE-WSW maximum horizontal compression [*Plumb and Cox*, 1987; *Evans*, 1989; *Zoback and Zoback*, 1989]. The correlation of R_h with elastic stiffness of the strata suggests that bed-to-bed stress variation results from a uniform ENE-WSW crustal straining. These stresses are superimposed on "remnant" stresses arising from a reduction of a paleo-overpressure or a WNW directed Alleghanian compression. *Evans* [1989] has reported evidence for a regional discontinuity in the depth trend of least stress ratio that coincides with the subsurface location of the Silurian Salina salt. He proposed that high stress levels above the salt horizon represents a remnant stress arising from WNW directed Alleghanian compression. Although these additional components may be locally significant, it is the ENE-WSW oriented crustal shortening that gives rise to the dominant component of stress throughout the entire stratigraphic section as seen in the Wilkins and Auburn wells. An important implication of the Wilkins and Auburn data is that whatever the regional strain rate history may be, stress variations arising from bed-to-bed differences in elastic stiffness have not been fully relaxed.

Another consequence of our data is that simple gravitational loading models of horizontal stress cannot predict the observed bed-to-bed stress contrasts regardless of whether the mechanism coupling vertical stress into horizontal stress is linear elasticity or an inelastic process associated with the critical shear strength of sedimentary rock. Stress data from geologically younger and tectonically less active basins elsewhere in North America are generally consistent with gravitational loading models for generating horizontal stresses [*Warpinski et al.*, 1983; *Whitehead et al.*, 1986; *Thiercelin and Plumb*, 1991]. In these regions it appears that shales are closer to a near lithostatic state of stress. Regional differences in the nature of lithologic stress contrasts suggest that we can expect different mechanisms to control stress contrasts in different geologic settings. Perhaps different mechanisms apply to different lithologies in a single stratigraphic sequence. These data lead us to expect relaxed-state profiles in regions of active normal faulting such as the Gulf Coast. However, if there is active tectonic extension, an extensional horizontal strain term might be required to properly predict the stress magnitudes.

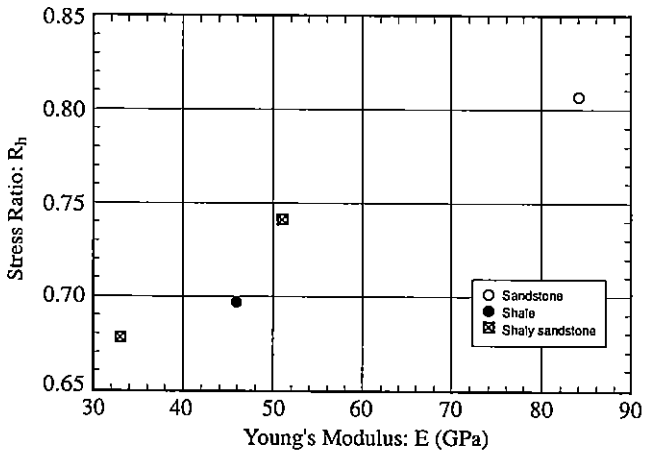

Fig. 17. Stress ratio R_h versus Young's modulus E in the Auburn well showing higher stress in rocks with higher modulus as expected from the horizontal elastic strain hypothesis. Notice the shale test; stress is better correlated with Young's modulus than rock type.

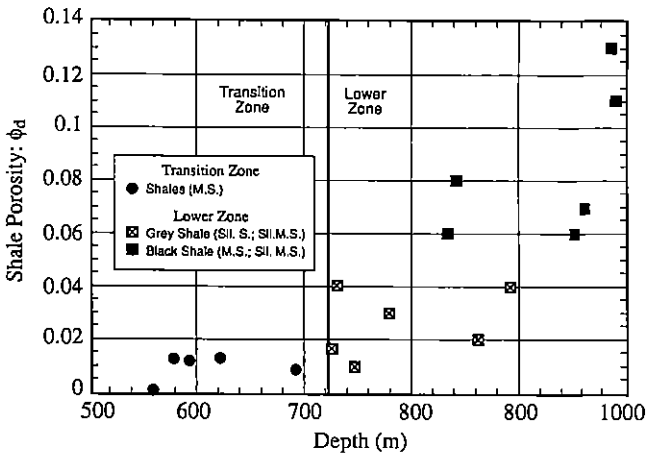

Fig. 18. Porosity of stress tested shales in the transition and lower zones of the Wilkins well. A line marks the location of the stress decrease at the base of the K sand. Porosity increases below the K sand in accord with the paleo-overpressure drainage hypothesis of *Evans et al.* [1989*b*].

This study has shown that shales are not always low strength rocks in a near lithostatic state of stress. Uniform horizontal strain, in regions of active compression, produces a stress profile across sand-shale or limestone-shale sequences which are unfavorable to hydraulic fracture containment by shales. Instead the sandstones may act as barriers to fractures nucleated in shales. This conclusion applies to natural extension fractures as well as hydraulic fractures created to stimulate low-permeability hydrocarbon reservoirs. We have also seen that shales are capable of sustaining significant levels of shear stresses (Table 2). These two facts indicate that the degree of diagenesis and the tectonic setting must be considered when assessing the fracture arresting characteristics of shales. In short, hydraulic fracture containment by shales is not guaranteed in regions of active compression.

CONCLUSIONS

Geophysical logs were used to identify and characterize the physical properties of strata where open hole stress measurements were made. Analysis of stress magnitudes and interval-averaged geophysical data showed that R_h is proportional to elastic stiffness and electrical resistivity and inversely proportional to clay content. These results were shown to be consistent with explanations of bed-to-bed stress variations proposed by *Evans et al.* [1989*b*] on the basis of core data from 20 km distant wells. The relationship between R_h and elastic stiffness is consistent with a regional horizontal strain leading to a compressed-state stress profile. A micromechanical interpretation of the load-bearing frame indicates that clays are the dominant load-bearing mineral in the shales, as expected. An increase in porosity was found at the base of the K sand in accord with the pore pressure drainage hypothesis for the large stress decrease recorded there. New results from the Auburn well show that the same uniform strain signal affects the entire Paleozoic stratigraphic section of New York State. This finding strengthens

our belief that lithologic stress variations in the northern Appalachian Basin are caused by an ENE-WSW directed uniform elastic strain acting on beds of different Young's modulus rather than by variations in rock shear strength. An important implication of the Wilkins and Auburn data is that regardless of the regional strain rate history, stress variations arising from differing elastic stiffness of beds have not fully relaxed.

This study has also shown that shales are not always low shear strength rocks in a near lithostatic state of stress. While a near lithostatic state applies to some shales, it does not apply to the northern Appalachian basin.

In regions of significant horizontal strain, rocks with the greatest elastic stiffness are likely to be barriers to hydraulic fracture propagation. In the northern Appalachian Basin, sandstone and limestones are likely barriers to fractures nucleated in shales.

APPENDIX: RELATIONS USED TO ESTIMATE ELASTIC MODULI AND BULK POROSITY

Elastic moduli. Elastic parameters are computed from compressional and shear wave velocities V_p and V_s and bulk density ρ_b obtained from the sonic and density logs using relations given below. We assume that the formation can be modeled as an isotropic elastic solid. To a first approximation, poroelastic effects can be ignored in these low-porosity rocks. Anisotropy may be important here but was neglected in the present analysis.

Shear modulus G

$$G = \rho_b V_s^2 \tag{A1}$$

Young's modulus E

$$E = \rho_b V_s^2 \left[\frac{3V_p^2 - 4V_s^2}{V_p^2 - V_s^2} \right] \tag{A2}$$

Bulk modulus K_b

$$K_b = \rho_b [V_p^2 - \tfrac{4}{3} V_s^2] \tag{A3}$$

Poisson's ratio ν

$$\nu = \left[\frac{V_p^2 - 2V_s^2}{2[V_p^2 - V_s^2]} \right]. \tag{A4}$$

Bulk porosity. The bulk density of a fluid saturated porous rock is given by

$$\rho_b = \phi_d \rho_f + (1 - \phi_d) \rho_{\text{ma}}, \tag{A5}$$

where the average density of the solid phase is ρ_{ma}, the average density of the pore fluid is ρ_f and ϕ_d is the volume fraction of pores or the bulk porosity. Bulk porosity is computed as

$$\phi_d = \frac{\rho_{\text{ma}} - \rho_b}{\rho_{\text{ma}} - \rho_f}, \tag{A6}$$

where we assume $\rho_{\text{ma}} = 2.75$ g/cm^3 and $\rho_f = 1.1$ g/cm^3.

Acknowledgments. Many people contributed to this research. We could not have done this work without help from the Northeast Division, which provided SDR with logging services. Rod Chambers, Bob Davis, and Chuck Davis were more than helpful. Bob Davis and Chuck Davis were able to find logging trucks just in the nick of time, which was no small task! Memorable sleepless nights were spent logging the Wilkins well with Paul Babasick and Fred Krampe. We greatly appreciate the assistance from Olive Liu, who did all of the digital sonic processing. Phil Fulla, Jim Wood, and Roy Dove helped pilot other data processing through logos and beyond. We acknowledge the useful and stimulating discussions with Darwin Ellis, Mike and Susan Herron, Pabitra Sen, and Jim Kent. Terry Engelder and Keith Evans were supported in part by a contract from the Morgantown Energy Technology Center DE-AC21-83MC20337 plus grants from EXXON and Schlumberger. We also wish to thank Steve Hickman and D. Moore for constructive comments in their reviews.

REFERENCES

Anderson, R. A., D. S. Ingram, and A. M. Zanier, Fracture pressure gradient determination from well logs, paper presented at 47th Annual Fall Meeting, Paper 4135, Soc. of Pet. Eng., San Antonio, Tex., Oct. 8–11, 1972.

Biot, M. A., Theory of propagation of elastic waves in a fluid saturated porous solid, *J. Acoust. Soc. Am.*, *28*, 168–178, 1956.

Breckels, I. M., and H. A. M. van Eekelen, Relationship between horizontal stress and depth in sedimentary basins, *J. Pet. Technol.*, *34*, 2191–2199, 1982.

Clavier, C., G. Coates, and J. Dumanoir, Theoretical and experimental bases for the dual-water model for interpretation of shaly sands, *Soc. Pet. Eng. J.*, *24*, 153–167, 1984.

Ellis, D. V., *Well Logging For Earth Scientists*, 532 pp., Elsevier, New York, 1987.

Engelder, T., Loading paths to joint propagation during a tectonic cycle: An example from the Appalachian Plateau, U.S.A., *J. Struct. Geol.*, *7*(3/4), 459–476, 1985.

Engelder, T., and P. Geiser, On the use of regional joint sets as trajectories of paleostress fields during the development of the Appalachian Plateau, New York, *J. Geophys. Res.*, *85*, 6319–6341, 1980.

Engelder, T., and G. Oertel, Correlation between abnormal pore fluid pressure and tectonic jointing in the Devonian Catskill delta, *Geology*, *13*, 863–866, 1985.

Ettensohn, F. R., The Catskill delta complex and the Acadian orogeny, a model, in The Catskill Delta, *Spec. Pap. Geol. Soc. Am.*, *201*, 39–49, 1985.

Evans, K. F., Appalachian stress study, 3, Regional scale stress variations and their relation to structure and contemporary tectonics, *J. Geophys. Res.*, *94*, 17,619–17,645, 1989.

Evans, K. F., and T. Engelder, A study of stress in Devonian shales of the Appalachian Plateau, DOE final report to contract DE-AC21-83MC20337, Morgantown Energy Technol. Cent., Morgantown, W. Va., 1987.

Evans, K. F., and T. Engelder, Some problems in estimating horizontal stress magnitudes in "thrust" regimes, *Int. J. Rock Mech. Min. Sci.*, *26*, 647–660, 1989.

Evans, K. F., T. Engelder, and R. A. Plumb, Appalachian stress study, 1, A detailed description of in situ stress variations in Devonian shales of the Appalachian Plateau, *J. Geophys. Res.*, *94*, 7129–7154, 1989*a*.

Evans, K. F., G. Oertel, and T. Engelder, Appalachian stress study, 2, Analysis of Devonian shale core: Some implications for the nature of contemporary stress variations and Alleghanian deformation in Devonian rocks, *J. Geophys. Res.*, *94*, 7154–7170, 1989*b*.

Frisinger, M., and R. E. Cooper, Techniques for quantifying formation stress and fracture fluid response for optimum hydraulic fracture design, paper presented at Offshore Europe 85 Conference, paper 14015, Soc. of Pet. Eng., Aberdeen, England, Sept. 10–13, 1985.

Gassmann, F., Über die Elastizität poröser Medien, *Vierteljahresschr. Naturforsch. Ges. Zurich*, *96*, 1–23, 1951.

Geertsma, J., Velocity-Log Interpretation: The Effect of Rock Bulk Compressibility, *Soc. Pet. Eng. J.*, *222*, 235–248, 1961.

Haimson, B. C. Crustal stress in the continental United States as derived from hydrofracturing tests, in *The Earth's Crust, Geophys. Monogr. Ser.*, vol. 20, edited by J. G. Heacock, pp. 576–592, AGU, Washington, D. C., 1977.

Hickman, S. H., J. H. Healy, and M. D. Zoback, In situ stress, natural fracture distribution, and borehole elongation in the Auburn geothermal well, Auburn, New York, *J. Geophys. Res.*, *90*, 5497–5512, 1985.

Jaeger, J. C., and N. G. W. Cook, *Fundamentals of Rock Mechanics*, 2nd ed., John Wiley, New York, 1976.

Johnson, D. L., Evaluating S_h with Biot's poroelastic theory, *Tech. Rev.*, *34*(3), 24–25, 1986.

Kry, R. P., and J. M. Gronseth, In-situ stresses and hydraulic fracturing in the deep basin, *J. Can. Pet. Technol.*, *22*, 31–35, 1983.

Nolte, K. G., Fracture design considerations based on pressure analysis, paper presented at Cotton Valley Symposium, paper 10911, Soc. of Pet. Eng., Tyler, Tex., May 20, 1982.

Plumb, R. A., and J. Cox, Stress directions in eastern North America determined to 4.5 km from borehole elongation measurement, *J. Geophys. Res.*, *92*, 4805–4816, 1987.

Plumb, R. A., and S. M. Luthi, Analysis of borehole images and their application to geologic modeling of an eolian reservoir, *SPE Form. Eval.*, *4*, 505–514, 1989.

Plumb, R. A., and J. Singer, Insights into the mechanical properties of tight formations: A study of in-situ stress and fracture distribution at Auburn, New York, final report, 26 pp., N. Y. State Energy Res. and Dev. Auth., Albany, 1983.

Plumb, R. A., K. F. Evans, and T. Engelder, Correlation of mechanical properties and in-situ stress contrasts, *Eos Trans. AGU*, *68*(27), 627, 1987.

Sen, P. N., Electrochemical Origin of Conduction in Shaly Formations, paper presented at 62nd Annual Fall Technical Conference, Soc. Pet. Eng., Dallas, Tex., Sept. 27–30, 1987.

Simonson, E. R., A. S. Abou-Sayed, and R. J. Clifton, Containment of massive hydraulic fractures, *Soc. Pet. Eng. J.*, 27–32, 1978.

Smith, M. B., Stimulation design for short precise hydraulic fractures, *Soc. Pet. Eng. J.*, *25*, 371–379, 1985.

Thiercelin, M. J., and R. A. Plumb, A core based prediction of lithologic stress contrasts in east Texas formations, paper presented at Joint Rocky Mountain Regional Meeting and Low Permeability Reservoirs Symposium, paper 21847, Soc. of Pet. Eng., Denver, Colo., April 15–17, 1991.

Van Tyne, A., Subsurface Expression and Gas Productivity of Devonian Black Shales in Western New York, in *The Geology of Northern Appalachian Basin: Fieldguide to the 54th Annual Meeting*, edited by E. J. Buehler, and P. E. Calkin, pp. 371–385, New York State Geological Association, Hempstead, 1982.

Warpinski, N. R., Elastic and viscoelastic calculations of stresses in sedimentary basins, paper presented at Unconventional Gas Technology Symposium, paper 15243, Soc. of Pet. Eng., Louisville, Ky., May 18–21, 1986.

Warpinski, N. R., R. A. Schmidt, and D. A. Northrop, In-situ stresses: The predominant influence on hydraulic fracture containment, *J. Pet. Technol.*, *34*, 653–664, 1982.

Warpinski, N. R., P. Branagan, and R. Wilmer, In-situ stress measurements at DOE's Multiwell Experiment site, Mesa Verde Group, Rifle, CO, paper presented at 58th Annual Technical Meeting, paper 12142, Soc. of Pet. Eng., San Francisco, Calif., Oct. 5–8, 1983.

Waxman, M. H., and L. J. M. Smits, Electrical conductivities in oil-bearing shaly sands, *Soc. Pet. Eng. J.*, *8*, 107–122, 1968.

Wedel, A. A., Geologic structure of the Devonian strata of south central New York, *N. Y. State Mus. Bull.*, *294*, 75 pp., 1932.

Whitehead, W. S., E. R. Hunt, R. J. Finley, and S. A. Holditch, In-situ stresses: A comparison between log derived values and actual field measured values in the Travis Peak Formation of east Texas, paper presented at Unconventional Gas Technology Symposium, paper 15209, Soc. of Pet. Eng., Louisville, Ky., May 18–22, 1986.

Zoback, M. L., and M. D. Zoback, Tectonic stress field in the continental U.S., in Geophysical Framework of the United States, edited by L. Pakiser and W. Mooney, *Mem. Geol. Soc. Am.*, *172*, 523–539, 1989.

T. Engelder, Department of Geosciences, Penn State University, University Park, PA 16802.

K. F. Evans, Institute of Geophysics, Swiss Federal Institute of Technology, ETH-Honggerberg, CH8093 Zurich, Switzerland.

R. A. Plumb, Schlumberger-Doll Research, Interpretation Sciences, Old Quarry Road, Ridgefield, CT 06877-4108.

(Received April 30, 1990;
revised February 28, 1991;
accepted March 22, 1991.)